iScience

Article

Dual-action thioarylamide-based small molecules to target drug-resistant bacteria and chronic inflammation

Graphical abstract

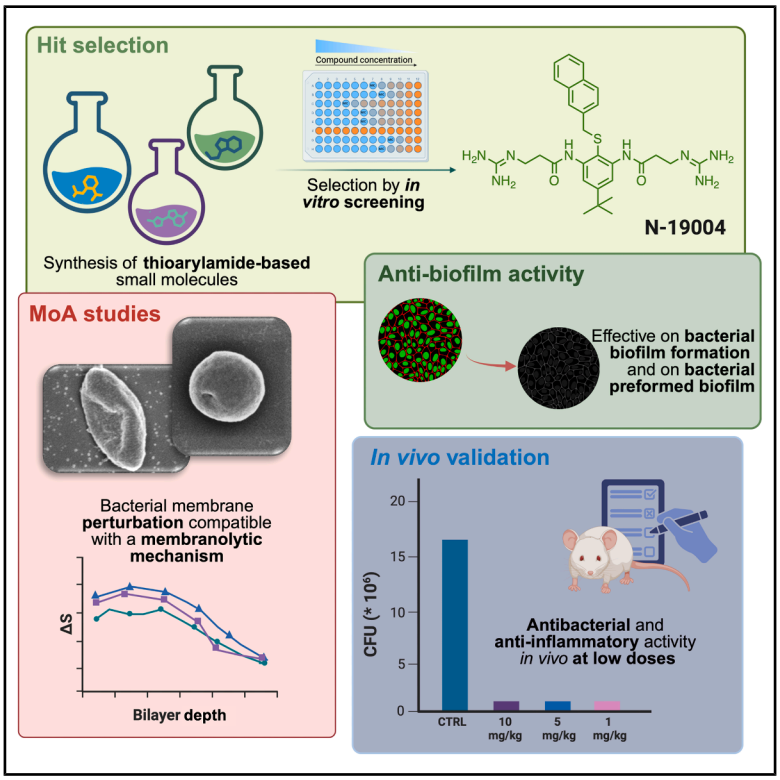

Highlights

- A library of thioarylamide-based compounds is active against MDR bacterial strains
- N-19004 is active in biofilm growth inhibition and disruption
- N-19004 significantly reduces *in vivo* bacterial burden and inflammation at low doses
- MoA studies suggest that the N-19004 antibacterial effect is linked to membrane disruption

Authors

Maria De Fenza, Rosa Gaglione, Alice Rossi, ..., Angela Arciello, Vincenzo Pavone, Daniele D'Alonzo

Correspondence

dandalonzo@unina.it

In brief

Natural sciences; Biological sciences; Biochemistry; Microbiology

De Fenza et al., 2025, iScience *28*, 113674
November 21, 2025
https://doi.org/10.1016/j.isci.2025.113674

CellPress

iScience

CellPress
OPEN ACCESS

Article

Dual-action thioarylamide-based small molecules to target drug-resistant bacteria and chronic inflammation

Maria De Fenza,[1] Rosa Gaglione,[1] Alice Rossi,[2] Marco Campanile,[1] Angela Cesaro,[1,3] Davide Gugliandolo,[2] Ida De Fino,[2] Marco Chino,[1] Luigi Petraccone,[1] Angelina Lombardi,[1] Gerardino D'Errico,[1] Alessandra Bragonzi,[2] Angela Arciello,[1] Vincenzo Pavone,[1] and Daniele D'Alonzo[1,4,*]

[1]Department of Chemical Sciences, University of Naples Federico II, 80126 Naples, Italy

[2]Infections and Cystic Fibrosis Unit, Division of Immunology, Transplantation and Infectious Diseases, IRCCS San Raffaele Scientific Institute, 20132 Milano, Italy

[3]Present address: University of Pennsylvania, Philadelphia, PA, USA

[4]Lead contact

*Correspondence: dandalonzo@unina.it

https://doi.org/10.1016/j.isci.2025.113674

SUMMARY

We report the synthesis and the antibacterial activity of a library of thioarylamide derivatives, which include N-19004, previously developed as Formyl Peptide Receptor 1 antagonist. These compounds were active against a broad spectrum of pathogens, including clinical strains of *Staphylococcus aureus* and *Pseudomonas aeruginosa*. N-19004 and its analog N-19004-S were proficient in biofilm growth inhibition and disruption. In a murine model of chronic *Pseudomonas aeruginosa* lung infection, N-19004 significantly reduced bacterial burden and inflammation at low doses. As revealed by Electron Paramagnetic Resonance and Scanning Electron Microscopy analyses, the antibacterial effect of N-19004 mainly derives from its interference with the bacterial membrane bilayer. The formation of long filamentous cells was also observed. With its structural simplicity, good *in vivo* tolerability, and simultaneous antibacterial and anti-inflammatory activity, N-19004 emerges as a promising candidate for treating multi-drug resistant infections, particularly in cystic fibrosis-related lung disease, where chronic inflammation plays an important role.

INTRODUCTION

Although antibiotics represent a major advancement in human healthcare, their widespread and unregulated use has accelerated the emergence of antibiotic resistance, which currently poses a serious threat to global health.[1,2] The vast majority of drug-resistant infections so far identified in healthcare settings can be attributed to a specific group of pathogens, referred to as the "ESKAPE" organisms (*Enterococcus faecium*, *Staphylococcus aureus*, *Klebsiella pneumoniae*, *Acinetobacter baumannii*, *Pseudomonas aeruginosa*, and the *Enterobacter* species).[3,4] These pathogens share a repertoire of intrinsic or acquired resistance determinants,[5] enabling them to circumvent the bactericidal effects of antibiotics. As a result, a progressive reduction of antimicrobial efficacy occurs over time, which requires the combined and long-term use of antibiotics to achieve eradication.[6] Among ESKAPE bacteria, the most prevalent and persistent pathogens responsible for chronic infections, *Staphylococcus aureus* and *Pseudomonas aeruginosa* currently represent "high priority" microorganisms, necessitating the urgent development of novel therapies, because of the emergence of multidrug-resistant (MDR) isolates against the most commonly used antibiotics, including aminoglycosides (tobramycin, gentamicin, amikacin), fluoroquinolones (ciprofloxacin), and β-lactams (ceftazidime, meropenem, imipenem, and so forth).[7,8] *Staphylococcus aureus* and *Pseudomonas aeruginosa* are also the most prevalent and persistent pathogens responsible for chronic lung infections, especially in people affected by cystic fibrosis (CF).[9] CF is a life-threatening genetic disease that primarily affects the respiratory system. The Cystic Fibrosis Transmembrane Conductance Regulator (CFTR) is the causative gene of the disease and leads to impaired chloride transport, resulting in abnormal thick mucus production in the lungs.[10] The mucus creates an ideal breeding ground for bacterial colonization,[11] which contributes to epithelial surface damage and airway plugging with a general deterioration of lung tissues, eventually resulting in a pulmonary function decline. If inadequately managed, bacterial infections in CF can elicit chronic inflammation, further contributing to lung deterioration and fibrosis.[12] This inflammatory cycle not only worsens respiratory functions but also reduces the efficacy of antibiotics by creating a hostile microenvironment that further supports bacterial persistence. Among patients with CF with *Staphylococcus aureus* and *Pseudomonas aeruginosa* infections, a significant proportion have been found to harbor MDR strains.[11] Drug therapies of CF-related *Staphylococcus aureus* and *Pseudomonas aeruginosa*-triggered infections rely on a

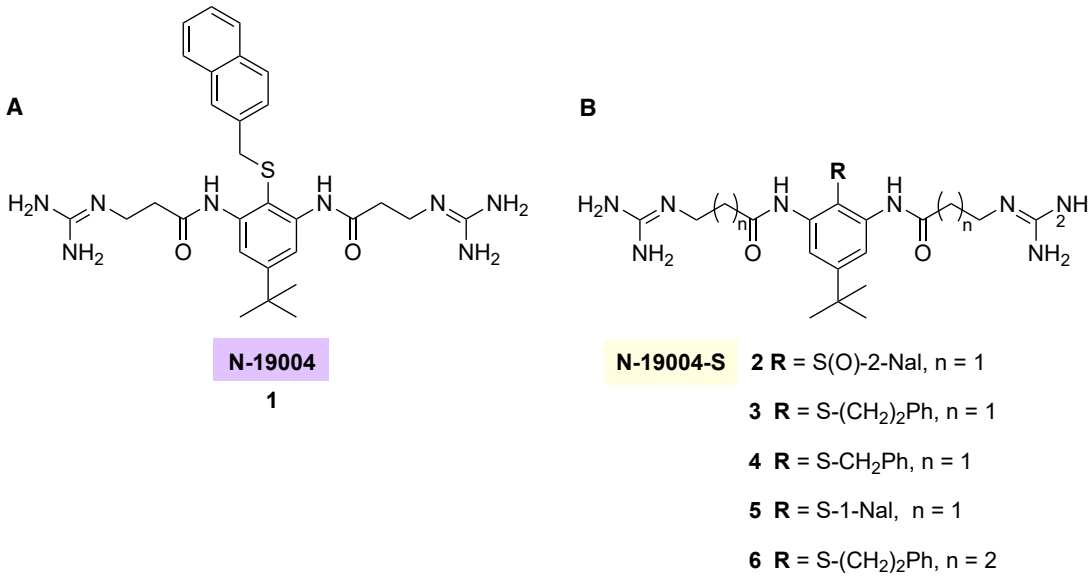

Figure 1. Thioarylamide-based small molecules

Chemical structures of (A) N-19004 (**1**; previously synthesized) and (B) of its new structural congeners **2–6**, tested in this work as potential antibacterial agents.

combination of multiple drugs, including antibiotics (e.g., tobramycin, aztreonam, azithromycin, fosfomycin, amoxicillin, cefazolin, vancomycin) and anti-inflammatory agents (e.g., corticosteroids, ibuprofen, leukotriene modifiers).[11] In contrast, only a few examples of drugs able to fight both infections and inflammation have been reported so far.[13–15] Some antibacterial drugs (e.g., ciprofloxacin) display an indirect anti-inflammatory effect.[16] Some anti-inflammatory drugs (e.g., fluticasone and ibuprofen) and modulators (e.g., ivacaftor, lumacaftor, and tezacaftor) have indirect effects on infections, by improving the overall respiratory environment.[17] Thus, the identification of dual-action drugs simultaneously reducing bacterial load while mitigating chronic inflammation is expected to represent a significant advancement in this field. On one hand, the use of a single drug for two therapeutic purposes would eliminate drug-drug interactions, enhancing treatment adherence and the overall efficacy of therapeutic protocols. On the other hand, the use of multifaceted therapeutics would reduce drug resistance phenomena, while mitigating adverse effects associated with a prolonged drug use.[18]

N-19004 (**1**, Figure 1A) was previously identified through a structure-based design approach aimed at discovering antagonists of Formyl Peptide Receptor 1 (FPR1).[19] The latter is a key regulator of cell migration, whose dysregulation has been implicated in chronic inflammatory pathologies.[20,21] The biological properties of N-19004 rely on the key presence of a central thioarylamide (2,6-diamido-4-*t*-butyl-thiophenyl) scaffold, required for proper molecular recognition to FPR1 by mimicking the bioactive turn conformation of the Arg-Aib-Arg segment in the parent bioactive peptide UPARANT.[22,23] The structural optimization of N-19004 was guided by molecular docking studies targeting the binding site of human FPR1 (hFPR1), exploiting high-confidence structural predictions from the AlphaFold2 database.[19] The experimental modulation by N-19004 of FPR1-mediated biological functions was then validated both *in vitro*[19] and in a mouse model of Age-related Macular Degeneration (AMD).[19]

In this study, the amphiphilic structure of N-19004, built around the central thioarylamide scaffold flanked by two positively charged ω-guanidino groups, prompted us to investigate its antimicrobial properties. This structural motif, while common among cationic antimicrobial peptides (CAMPs),[24,25] also shares notable structural homology with the arylamide-based foldamers developed by DeGrado et al.,[26] which demonstrated significant bactericidal efficacy via membrane disruption mechanisms, thus highlighting the therapeutic potential of this architecture. To investigate whether the antibacterial properties of the foldamers could be kept even in a minimal structure, a comprehensive antimicrobial evaluation of N-19004 was carried out. A mini-library of structural congeners (Figure 1B), including **2–6**, has also been synthesized and assayed to identify the hit molecule endowed with the most promising antimicrobial profile. The initial screening has encompassed a broad spectrum of bacterial pathogens. Special attention has been given to *Pseudomonas aeruginosa* and *Staphylococcus aureus* strains, focusing on their multi-drug resistant (MDR) variants - namely, methicillin-resistant *Staphylococcus aureus* (MRSA)[8] and the highly virulent *Pseudomonas aeruginosa* strain RP73,[24] both standing as clinical isolates from patients with CF. Following a thorough antimicrobial assessment of the most promising candidates, a mouse model of chronic lung *Pseudomonas aeruginosa* infection and inflammation has been used to validate the *in vivo* efficacy as an antibacterial agent while concurrently exerting its anti-inflammatory potential as FPR1 antagonist. As the final aim of this work, a candidate with a dual action as an antimicrobial and anti-inflammatory agent has been identified, potentially acting as a valuable weapon against difficult-to-treat infections, including those occurring in CF, where chronic inflammation plays an important role.

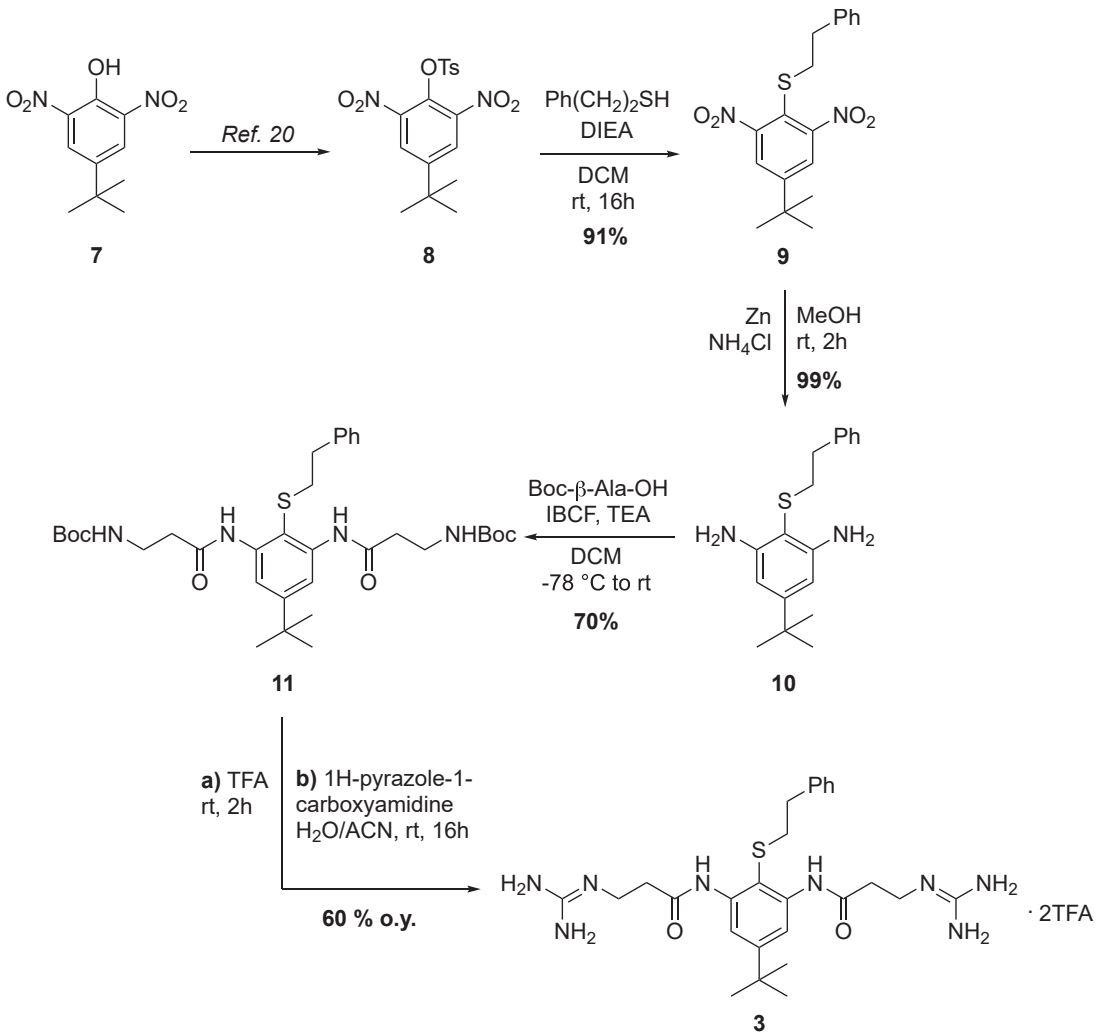

Scheme 1. Synthetic procedure used to prepare compound 3

RESULTS

Chemical synthesis

The synthetic route previously developed for the preparation of N-19004 (**1**),[19] recalling the procedure reported by Choi et al.,[27] was herein adapted for the synthesis of **3**, as shown in Scheme 1. When the synthetically available[19] tosyl ester **8** (from 4-*t*-butyl-2,6-dinitrophenol (**7**)) was coupled with 2-phenylethanethiol, the conversion of the latter into the corresponding thioether **9** was achieved in high yield (91%). The reduction of both nitro groups of **9** (Zn, NH_4Cl, MeOH) quantitatively afforded **10**, which was engaged in a double coupling reaction with two Boc-β-Ala-OH units. Under common conditions (IBCF, TEA), *bis*-amide **11** was obtained in 70% yield. Eventually, removal of *N*-Boc groups (TFA) and subsequent derivatization of the resulting amino groups with 1H-pyrazole-1-carboxamidine yielded the desired **3** as a *bis*-trifluoroacetate salt (60%).

Appropriate choice of the starting thiol enabled the synthesis of other N-19004 congeners (Scheme 2). Coupling reactions of tosyl ester **8** with phenylmethanethiol, 2-phenylethanethiol, or 1-naphthalenemethanethiol[28,29] allowed their conversion into the corresponding thioethers **9** or **12–13**, respectively (88–92%). In the effort to reduce the number of synthetic steps, a different path was then followed (Scheme 2). As *bis*-amines **10** and **14–15** were obtained by nitro group reduction (>99%), they were directly coupled (HBTU, HOBt, DIEA)[30,31] with β-aminopropionic acid or γ-aminobutyric acid, both pre-functionalized[32,33] with *bis*-Boc guanidine moieties. As the coupling products were formed, they were used as crude in the final deprotection step (TFA/TIS/H_2O) to afford compounds **4–6** (Scheme 2). Following this procedure, the coupling reactions provided the corresponding amides in good yields (70–76%).

By treating N-19004 (**1**) with an excess of hydrogen peroxide, we also prepared its sulfoxide derivative N-19004-S (**2**; Scheme 3), to elucidate the impact of sulfur oxidation on antimicrobial activity.

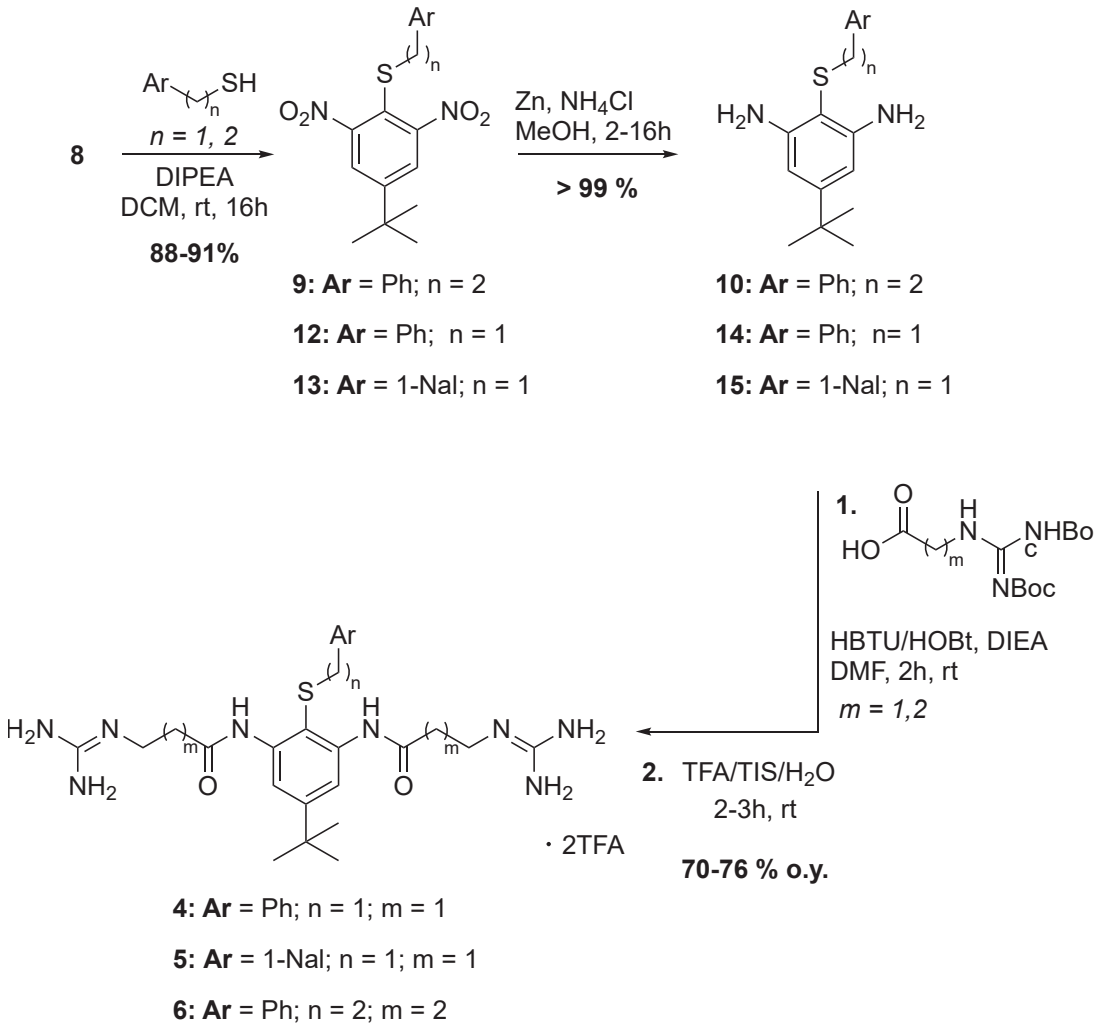

Scheme 2. Synthetic procedures used to prepare compounds 4-6

In vitro antimicrobial studies

MIC and MBC determination

The antimicrobial activity of N-19004 and its congeners was evaluated against *Pseudomonas aeruginosa* reference PAO1 and clinical strains RP73, AA2, and KK27, as well as against a plethora of other bacterial pathogens, including *Burkholderia cenocepacia* LMG 18863 and J2315, *Burkholderia multivorans* LMG 17582, *Enterococcus faecalis* ATCC 29212, *Straphylococcus aureus* ATCC 12600 and ATCC 29213, methicillin-resistant *Straphylococcus aureus* WKZ-2, *Salmonella enterica* ATCC 14028 and *Acinetobacter baumanii* ATCC 19606.

The broth microdilution method[34–38] was used to determine the minimal inhibitory concentration (MIC) values (the lowest compound concentrations able to completely inhibit bacterial growth) and the minimal bactericidal concentration (MBC) values (the lowest compound concentrations able to completely kill bacterial cells). Fosfomycin was employed as a positive control, as it demonstrated broad antibacterial activity against both Gram-positive and Gram-negative pathogens.[39] All tested compounds exhibited antibacterial activity, with MIC values ranging from 12.5 to 200 μM against the majority of tested bacterial strains (Table 1). Most compounds exhibited MIC and MBC values significantly lower than Fosfomycin. Among these, N-19004 and N-19004-S emerged as the most effective candidates, showing potent activity against nearly all tested bacterial strains, including the clinically isolated (Table 1).

Haemolytic activity

The release of hemoglobin from human erythrocytes was tested upon incubation with compounds **1–6**, to evaluate possible adverse haemolytic activity. To this aim, human red blood cells (hRBCs) were incubated with increasing concentrations (12.5–200 μM) of thioarylamide derivatives for 1 h at 37 °C. As shown in Figure S13, no lytic effects were observed within the range 12.5–200 μM when hRBCs were incubated with all compounds.

Time-kill kinetic assays

Further *in vitro* studies were then performed on the most promising compounds, N-19004 and N-19004-S, starting from a kinetic evaluation of the antimicrobial properties (Figure 2).

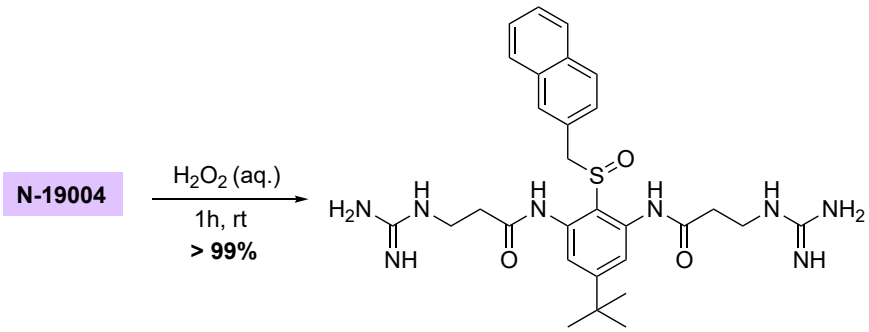

Scheme 3. Synthetic approach used to prepare N-19004-S (2) by the oxidation of N-19004 (1)

N-19004 and N-19004-S were analyzed in time-kill kinetic assays using both *Pseudomonas aeruginosa* KK27 and *Pseudomonas aeruginosa* RP-73 as Gram-negative bacterial strains, and *Staphylococcus aureus* ATCC 12600 and methicillin-resistant *Staphylococcus aureus* WKZ-2 as Gram-positive strains. As shown in Figure 2A, both *Staphylococcus aureus* ATCC 12600 and *Staphylococcus aureus* WKZ-2 were completely killed within 1–3 h upon treatment with either compound. A similar result was also obtained on *Pseudomonas aeruginosa* strains (Figure 2B), as they were killed within 2h.

Antibiofilm properties

Both methicillin-resistant *Staphylococcus aureus* and MDR *Pseudomonas aeruginosa* strains can form biofilms. Importantly, their biofilm forming activity is often associated with their multidrug-resistance profile.[40,41] To verify whether N-19004 and N-19004-S are endowed with anti-biofilm properties, crystal violet assays were first performed by testing clinically relevant bacterial pathogens, the same already identified for the time-killing experiments. N-19004 and N-19004-S demonstrated a significant ability to inhibit biofilm formation (40–50%) in the case of both Gram-negative and Gram-positive strains at concentrations much lower than those needed to directly kill planktonic bacterial cells (Figures 3A and 3B).

To further investigate the anti-biofilm formation activity of the N-19004 and N-19004-S, confocal laser scanning microscopy (CLSM) analyses were also performed. As reported in Figures 4, S14, and S15, both compounds were found to significantly alter the biofilm architecture, reducing the biofilm biovolume of all tested strains at sub-MBC concentrations (25–50 μM in the case of Gram-negative strains and 6.25–12.5 μM in the case of Gram-positive strains). Both N-19004 and N-19004-S were found to determine from 2- to 3-fold reduction of biofilm biovolume in the case of *Pseudomonas aeruginosa* RP73 (Figure 4) and *Pseudomonas aeruginosa* KK27 (Figure S15) when tested at 50 μM, whereas only N-19004 was found to achieve a 3-fold reduction of biofilm biovolume in the case of methicillin-resistant *Staphylococcus aureus* WKZ-2 (Figure 5) and of *Staphylococcus aureus* ATCC 12600 (Figure S14). Furthermore, the LIVE/DEAD Bacterial Viability kit was employed to better investigate biofilm morphology before and after treatment with N-19004 and N-19004-S. In this assay, bacteria with intact membranes fluoresce green, while those with compromised membranes appear red. In contrast, fully

Table 1. MIC and MBC values (μM)

	1		2		3		4		5		6		Fosfomycin	
Bacterial strain	MIC	MBC	MIC	MBC	MIC	MBC	MIC	MBC	MIC	MBC	MIC	MBC	MIC	MBC
B. cenocepacia LMG 18863	>200	>200	50	100	25	100	>200	>200	>200	>200	>200	>200	1140	1140
B. multivorans LMG 17582	>200	>200	50	100	>200	>200	>200	>200	>200	>200	>200	>200	1140	1140
B. cenocepacia J2315	>200	>200	100	200	>200	>200	>200	>200	>200	>200	>200	>200	1140	1140
P. aeruginosa AA2	25	50[a]	50	100	25	100[a]	100	200[a]	50	200	100	200	1140	1140
P. aeruginosa PAO1	100	200[a]	50	100	50	100[a]	50	100[a]	50	200	100	200[a]	2280	2280
P. aeruginosa KK 27	25	200	25	50	50	200[a]	50	200[a]	50	200	50	200	2280	2280
P. aeruginosa RP 73	25	200	100	200	25	200[a]	50	200[a]	50	200	50	200	2280	2280
E. faecalis ATCC® 29212	100	200	100	200	>200	>200	>200	>200	100	200[a]	>200	>200	4340	4340
S.aureus ATCC® 12600	25	50	25	50	25	25	25	50	12.5	12.5	12.5	25	4340	4340
S. aureus ATCC® 29213	>200	>200	100	200	100	200[a]	>200	>200	>200	>200	>200	>200	4340	4340
S. aureus MRSA (WKZ-2)	12.5	25	25	50	25	50	25	50	12.5	25	25	50	4340	4340
S. enterica ATCC® 14028	>200	>200	>200	>200	100	200	>200	>200	>200	>200	>200	>200	4340	4340
A. baumannii ATCC® 19606	>200	>200	>200	>200	>200	>200	>200	>200	>200	>200	>200	>200	4340	4340

Antimicrobial activity was evaluated by testing concentrations of thioarylamide derivatives **1–6,** ranging from 0 to 200 μM, against 13 bacterial strains; reported data refer to assays carried out in triplicate.

[a]$MBC_{90\text{-}95}$ indicates that 90–95% of the cells die under the experimental conditions tested.

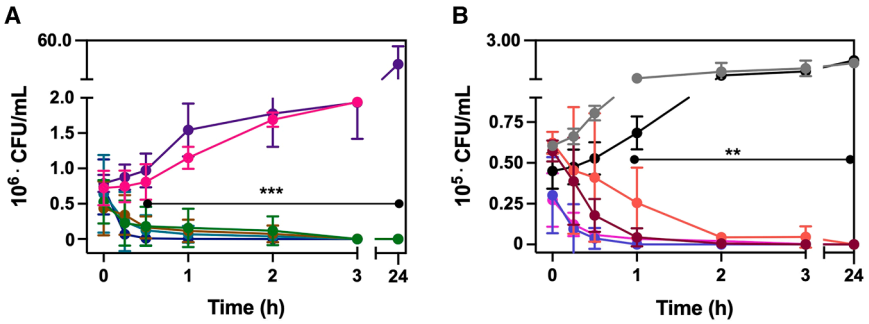

Figure 2. Time-kill kinetic assays

(A) *Staphylococcus aureus* ATCC 12600 (● control) and *methicillin-resistant Staphylococcus aureus* WKZ-2 (● control) treated with N-19004 and N-19004-S at their bactericidal concentrations (● *Staphylococcus aureus* ATCC 12600 treated with N-19004; ● *Staphylococcus aureus* ATCC 12600 treated with N-19004-S; ● *MRSA* treated with N-19004; ● *MRSA* treated with N-19004-S).(B) *Pseudomonas aeruginosa* KK27 (● control) and *Pseudomonas aeruginosa* RP73 (● control) treated with N-19004 and N-19004-S at their bactericidal concentrations (● *Pseudomonas aeruginosa* KK27 treated with N-19004; ● *Pseudomonas aeruginosa* KK27 treated with N-19004-S; ● *Pseudomonas aeruginosa* RP73 treated with N-19004; ● *Pseudomonas aeruginosa* RP73 treated with N-19004-S). In both cases, the time-kill kinetics have been compared with those obtained by incubating cells with only buffer and medium (control cells). Assays were carried out in duplicate, and the data represent the mean of the counts of three dilutions plated on TSA plates. Significant differences for treated versus control samples were assessed using the unpaired two-tailed Student's t test and indicated as follows: $^{**}p < 0.01$; $^{***}p < 0.001$.

lysed or dead cells are not detectable. The staining revealed clear morphological alterations in the biofilms following treatment, accompanied by an increased proportion of dead cells (Figures 4, S14, and S15).

The anti-biofilm activity of N-19004 and N-19004-S was also evaluated on preformed biofilms. As highlighted in Figure 5, the biofilm architecture was significantly modified for Gram-negative bacteria, and the strongest effect was observed on *Pseudomonas aeruginosa* KK27 biofilm (Figure 5A). N-19004 and N-19004-S were also observed to induce the growth of long filamentous cells, a phenomenon particularly pronounced in *Pseudomonas aeruginosa* RP73 (Figure 5B). This suggests that these compounds may interfere with cell division by inhibiting septation, as previously reported.[36,38] Weaker effects were detected when testing against Gram-positive bacteria (Figures S16 and S17). In this case, no significant effects were detected on biofilm biovolume.

Safety and efficacy in pre-clinical studies

Given the promising results from *in vitro* experiments, *in vivo* assays in a chronic *Pseudomonas aeruginosa* MDR-RP73 infection model[42–46] were performed. This murine infection model closely replicates the lung disease progression in patients with CF, and it is widely used as a valuable tool for both pathogenesis studies and the assessment of novel therapies.[42–47] We selected N-19004 over N-19004-S as the most suitable candidate for these studies, owing to the more positive results regarding the antibiofilm activity *in vitro*. Furthermore, N-19004 was well tolerated in murine models.[19] The experimental design for efficacy in pre-clinical studies is outlined in Figure S18. Immunocompetent C57BL/6NCrlBR male mice were challenged with a (1×10^6) of CFU of the MDR-RP73 strain, embedded in agar beads by intratracheal administration.[45] As these conditions are also associated with substantial lung inflammation,[48] the effect of N-19004 was then studied as either an anti-microbial and/or an anti-inflammatory agent. Daily subcutaneous injections of N-19004 were performed over seven days by the day of infection, using four different doses (1, 2.5, 5, and 10 mg/kg). The dosing regimen is based on a previous study, which was conducted in a murine model of AMD.[19] The results of the experiments are depicted in Figures 6 and 7. N-19004-treated mice showed a significant reduction in the bacterial burden at all tested doses, both in the lung and in the bronchoalveolar lavage fluid (BALF), compared to vehicle-treated mice (Figures 6A–6C). A plateau in the pharmacological effect was already reached at the lowest dose (1 mg/kg), as revealed by the CFU count in lungs and in the BALF (Figure 6). This

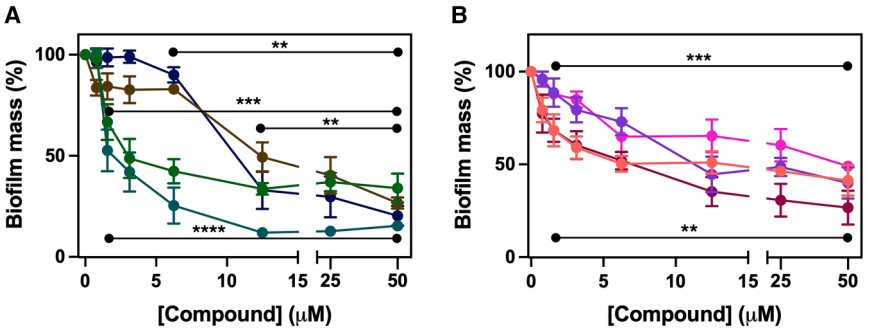

Figure 3. Inhibition of biofilm formation

(A) Anti-biofilm formation activity toward Gram-positive strains (● *Staphylococcus aureus* ATCC 12600 treated with N-19004; ● *Staphylococcus aureus* ATCC 12600 treated with N-19004-S; ● *MRSA* treated with N-19004; ● *MRSA* treated with N-19004-S).

(B) Anti-biofilm formation activity toward Gram-negative strains (● *Pseudomonas aeruginosa* KK27 treated with N-19004; ● *Pseudomonas aeruginosa* KK27 treated with N-19004-S; ● *Pseudomonas aeruginosa* RP73 treated with N-19004; ● *Pseudomonas aeruginosa* RP73 treated with N-19004-S). Data represent the mean (± standard deviation, SD) of at least three independent experiments, each one carried out with triplicate determinations. Significant differences for treated versus control samples were assessed using the unpaired two-tailed Student's t test and indicated as follows: $^{**}p < 0.01$; $^{***}p < 0.001$; or $^{****}p < 0.0001$.

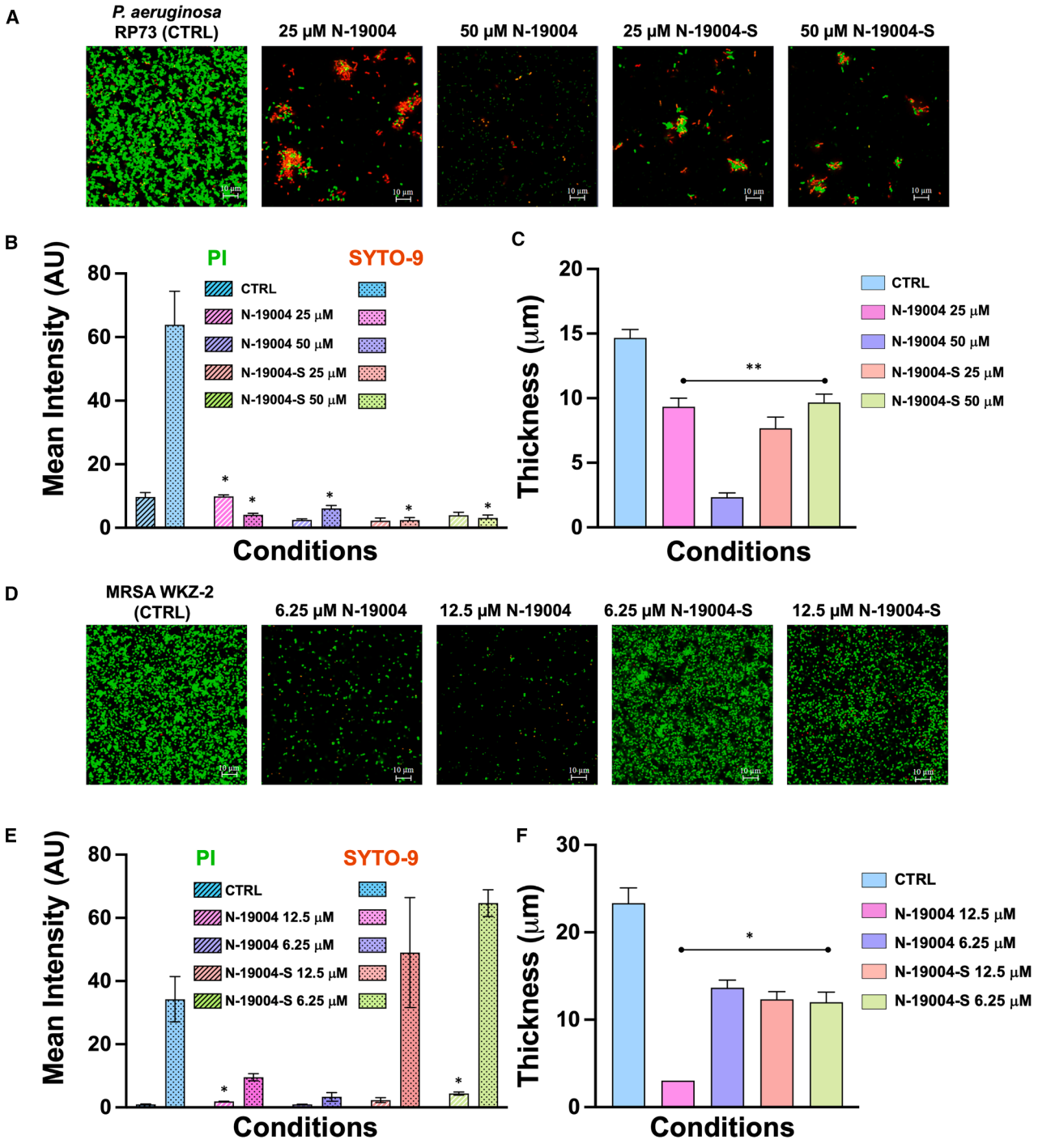

Figure 4. Inhibition of biofilm formation: CLSM analysis

Effects of N-19004 and N-19004-S on the biofilm formation of (A–C) *Pseudomonas aeruginosa* RP73 and (D–F) *Staphylococcus aureus* WKZ-2. (A) and (D): biofilm images collected by using a confocal laser scanning microscope (Zeiss LSM 710, Zeiss) and a 63X objective oil-immersion system. Two-dimensional structures of the biofilms were obtained by confocal z stack using Zen Lite 2.3 software. Cell viability within the biofilm structure was evaluated by staining with a LIVE/DEAD Bacterial Viability kit (SYTO-9 as green-fluorescent stain and Propidium Iodide (PI) as the red-fluorescent stain). (B) and (E): mean intensity graphs. (C) and (F): biovolume values (thickness), calculated by using Zen Lite 2.3 software. Confocal laser scanning microscopy (CLSM) analyses in static conditions were carried out by using ThermoScientific Nunc Lab-Tek Chambered Coverglass systems. Each experiment was performed in duplicate, and all images were taken under identical conditions. Significant differences (Student's t test) for treated versus control samples were indicated as follows: *, $p < 0.05$; **, $p < 0.01$.

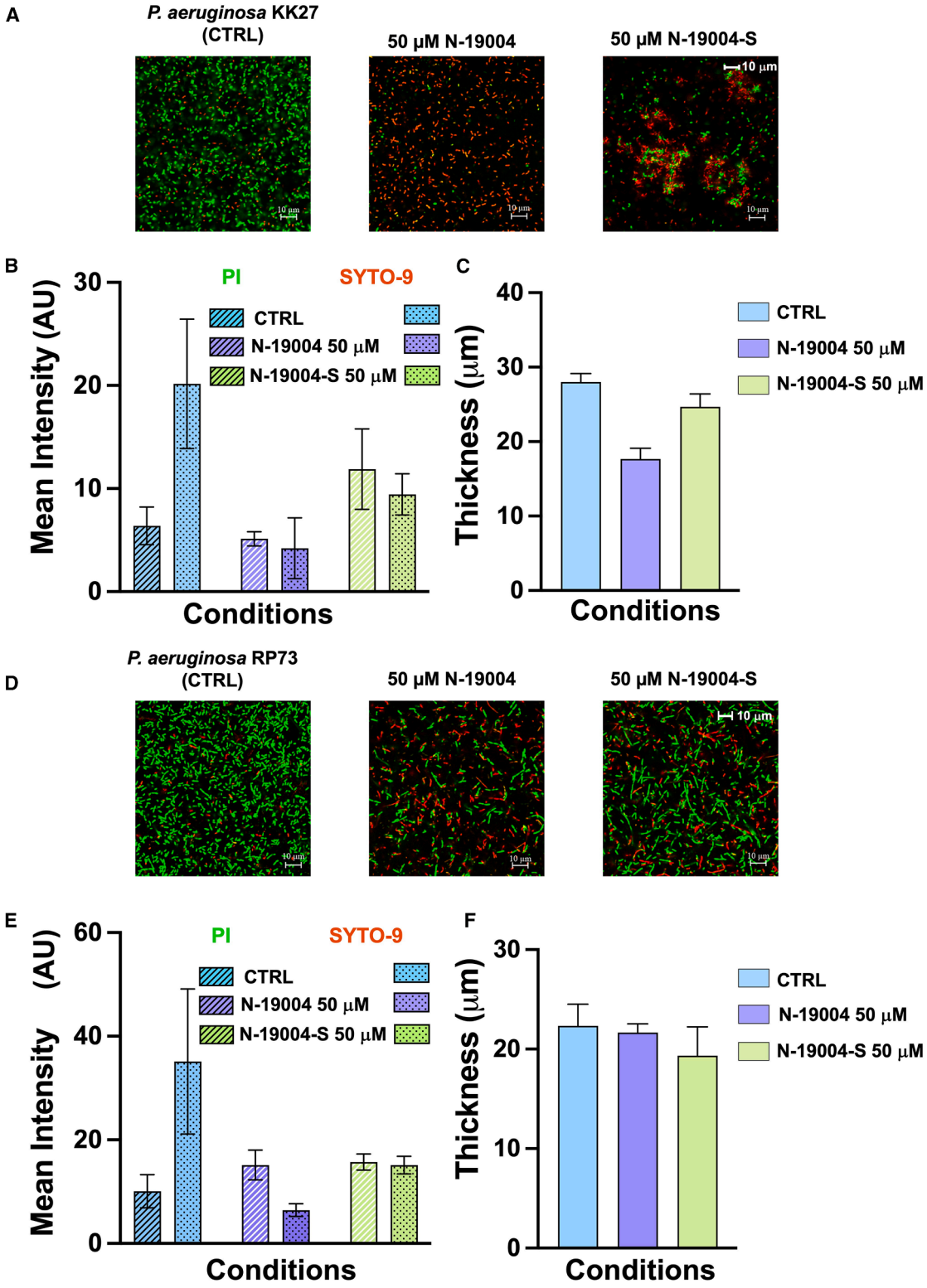

Figure 5. Inhibition of pre-formed biofilm: CLSM analysis

Effects of N-19004 and N-19004-S on pre-formed biofilm of (A–C) *Pseudomonas aeruginosa* KK27 and (D–F) *Pseudomonas aeruginosa* RP73. (A) and (D): biofilm images were collected by using a confocal laser scanning microscope (Zeiss LSM 710, Zeiss) and a 63X objective oil-immersion system. Two-dimensional structures of the biofilms were obtained by confocal z stack using Zen Lite 2.3 software. Cell viability within the biofilm structure was evaluated by staining with a

(legend continued on next page)

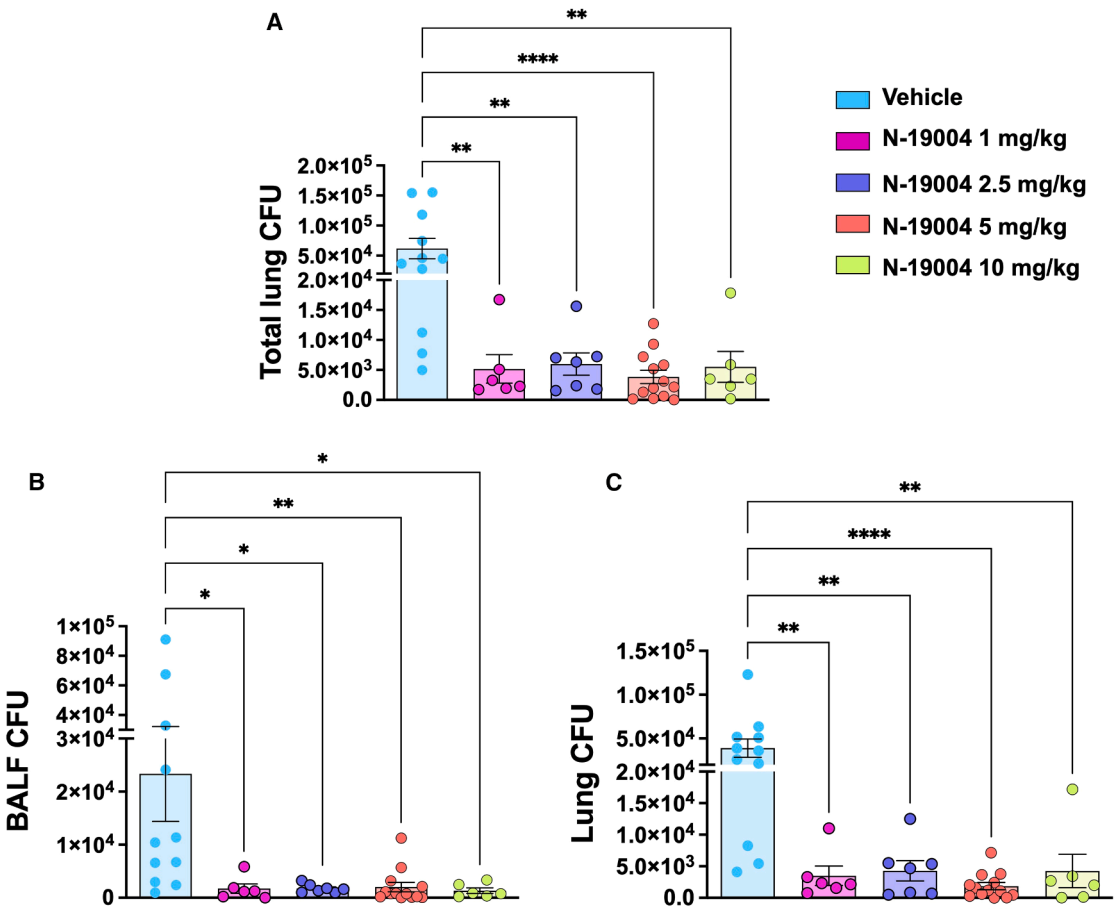

Figure 6. Effect of N-19004 on bacterial burden in a murine model of *Pseudomonas aeruginosa* chronic infection

C57Bl/6NCrlBR male mice were infected with *Pseudomonas aeruginosa* MDR-RP73 embedded in agar beads by intratracheal inoculation. Subcutaneous treatment with N-19004 1, 2.5, 5, and 10 mg/kg or vehicle (saline) was started soon after infection and continued daily for 7 days. (A) Total (lung+BALF), (B) BALF, and (C) lung *Pseudomonas aeruginosa* CFU upon treatment with N-19004. One way ANOVA with Dunnett's multiple comparison test: $*p < 0.05$, $**p < 0.01$, $***p < 0.001$, $****p < 0.0001$ vs. vehicle.

contributed to improving the general health status of mice, as revealed by the faster recovery of body weight observed in N-19004 treated mice compared to vehicle-treated mice (Figure S19). N-19004 treatment also significantly reduced total cell count and neutrophils in the BALF, indicating a reduction in the inflammation (Figures 7A–7C). Different from the antimicrobial effect, the reduction of lung inflammation exhibited a concentration-dependent behavior, with the highest effect at a relatively higher dose (10 mg/kg). This differential dose-response pattern between antimicrobial and anti-inflammatory effects suggests that they are not directly correlated. Importantly, at this dose, the neutrophil count was deeply reduced, while the number of macrophages was almost unchanged. This suggests an effective control of neutrophilic inflammation, which plays a key role as a first-line defense in CF.

Mechanistic studies

EPR experiments on bacterial model membranes

Efforts were finally focused on determining the mechanism of action underlying the antimicrobial activity of N-19004 and its congeners. As antimicrobial peptides typically exert their activity by interacting with bacterial membranes and disrupting their functions,[49,50] we performed a physicochemical investigation on N-19004 by EPR spectroscopy to assess its membranotropic properties and ability to destabilize lipid bilayers. To mimic the anionic surface charge of bacterial membranes, we initially selected the previously reported composition[51] POPC/POPG 80/20 mol/mol as a lipid bilayer model. For a closer resemblance of Gram-positive and Gram-negative bacterial membranes, we then used lipid bilayers enriched with lipoteichoic acid (LTA), as an essential component of the *Staphylococcus tabveus*

LIVE/DEAD Bacterial Viability kit (SYTO-9 as green-fluorescent stain and Propidium Iodide (PI) as the red-fluorescent stain). (B) and (E): mean intensity graphs. (C) and (F): biovolume values (thickness), calculated by using Zen Lite 2.3 software. Confocal laser scanning microscopy (CLSM) analyses in static conditions were carried out by using ThermoScientific Nunc Lab-Tek Chambered Coverglass systems. Each experiment was performed in duplicate, and all the images were taken under identical conditions.

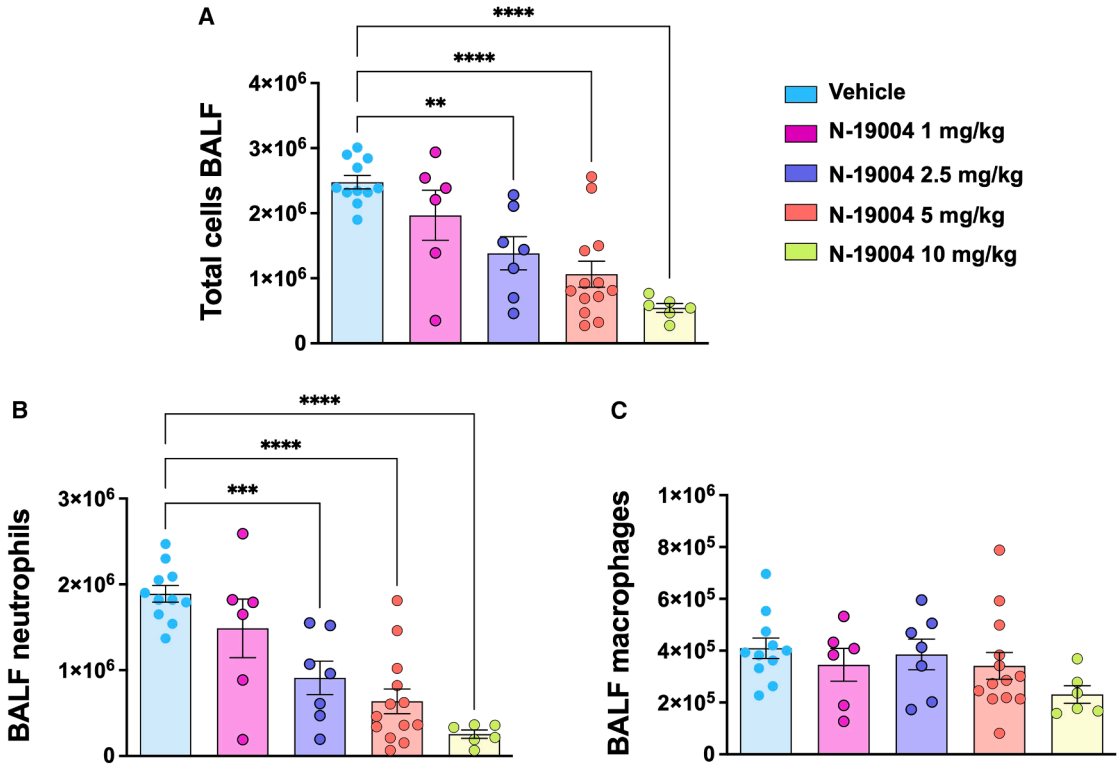

Figure 7. Effect of N-19004 on the inflammatory response in a murine model of *Pseudomonas aeruginosa* chronic infection

C57Bl/6NCrlBR male mice were infected with *Pseudomonas aeruginosa* MDR-RP73 embedded in agar beads by intratracheal inoculation. Subcutaneous treatment with N-19004 1, 2.5, 5, and 10 mg/kg or vehicle (saline) was started soon after infection and continued daily for 7 days. (A) Total cells in the BALF; (B) neutrophils in the BALF; (C) macrophages in the BALF. One way ANOVA with Dunnett's multiple comparison test: $^{*}p < 0.05$, $^{**}p < 0.01$, $^{***}p < 0.001$, $^{****}p < 0.0001$ vs. vehicle.

cell envelope,[52] and with lipopolysaccharides (LPS), to more accurately resemble the cell wall composition of *Pseudomonas aeruginosa*.[53] To evaluate whether structural perturbations were induced by N-19004 on bilayer regions, EPR spectra were acquired for 1-palmitoyl-2-stearoyl-(*n*-doxyl)-*sn*-glycero-3-phosphatidylcholine (*n*PC-SL) with n = 5, 7, 10, and 14, alternately embedded in liposomes (higher n values) and exposed to N-19004 (lower n values). A quantitative analysis of *n*PC-SL spectra furnished the acyl chain order parameter, S, a measure of the lipid local ordering in the segment to which the label is bound, and the isotropic hyperfine nitrogen constant a'_N, which provides information about the local polarity.[51] The parameters obtained from the *n*PC-SL spectra in POPC/POPG 80/20 bilayers and the preliminary effect of N-19004 on POPC/POPG bilayers are reported in Figure S20 and Table S1.

The comparative effects of N-19004 on lipid bilayers POPC/POPG 80/20 mol/mol, POPC/POPG/LPS 80/15/5 mol/mol/mol, and POPC/POPG/LTA 80/15/5 mol/mol/mol are reported in Figure 8. The addition of N-19004 to the POPC/POPG bilayer led to an increase of ΔS at all label positions, with the most significant change for 5PC-SL. This suggests that N-19004 enhances bilayer stiffness primarily by localizing at the surface, without penetrating the hydrophobic core. Further support was provided by the $\Delta a'_N$ values, indicating increased polarity in the shallow membrane region, as a result of the compound's positive charge (+2) and/or increased water penetration just below the membrane-water interface. In the presence of LPS and LTA, the ability of N-19004 to perturb the lipid bilayer increased. ΔS was higher at the shallower spin-label positions, revealing that N-19004 is able to interact with the membrane surface despite the presence of LPS and LTA bulky headgroups. On the contrary, the ability to perturb the membrane at the level of 14PC-SL was again reduced. The trend of $\Delta a'_N$ reflects that of ΔS, suggesting that the cationic N-19004 determines an increase of local polarity in the more external region of the lipid membrane.

Overall, the observed alterations in bilayer structure and dynamics in the presence of LPS and LTA indicate a detectable interaction of N-19004 with the bilayer surface and a consequent perturbation of the lipid local organization, compatible with a potential membranolytic mechanism underlying its antimicrobial activity.

Scanning Electron Microscopy

The effect of N-19004 on the morphology of bacterial cells was eventually explored by Scanning Electron Microscopy (SEM). SEM analyses were performed by testing N-19004 at 12.5 μM and 25 μM against *Staphylococcus aureus* MRSA (WKZ-2) and *Staphylococcus aureus* ATCC 12600, while at 25 μM and 50 μM in the case of *Pseudomonas aeruginosa* RP 73 and *Pseudomonas aeruginosa* KK 27. Representative pictures of

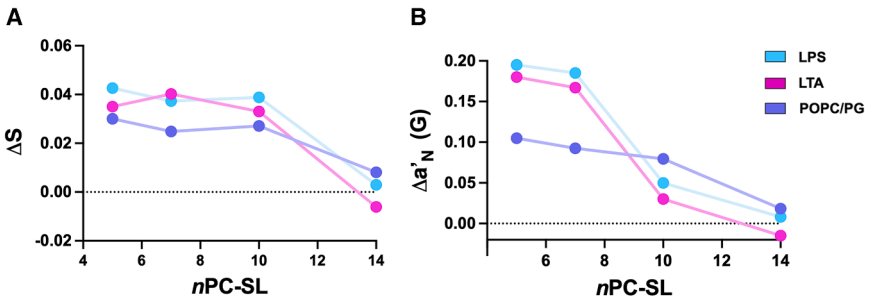

Figure 8. EPR analysis of bacterial model membranes

Values of (A) Δ*S* and (B) $\Delta a'_N$ for POPC/POPG (80/20 mol/mol, ●), POPC/POPG/LPS (80/15/5 mol/mol/mol, ●), and POPC/POPG/LTA (80/15/5 mol/mol/mol, ●) are reported as a function of *n* in *n*PC-SL, in the presence of N-19004. The variations of *S* and a'_N values have been calculated with respect to relative to those of POPG/POPC bilayers in the absence of N-19004. The circles indicate the experimental data points, while the lines are a guide for the eye.

the bacterial cells of *Pseudomonas aeruginosa* RP-73 and *Staphylococcus aureus* MRSA WKZ-2 upon treatment with N-19004 are reported in Figures 9 and 10 (the images of *Staphylococcus aureus* ATCC 12600 and *Pseudomonas aeruginosa* KK 27 treated cells are reported in ESI, Figures S24 and S25).

In the case of untreated control samples, intact and homogeneous cells were present (Figures 9 and 10, upper panels). Conversely, upon treatment with N-19004, in all bacterial strains, a progressive detachment of the cell wall appeared evident along with a significant cell lysis, which was found in a dose-dependent manner. Cell membrane permeabilization and cell shrinkage were manifest with a consequent well-noticeable leakage of the cytoplasmic content. After 16h of treatment, bacterial surfaces appear corrugated with some dimples, whereas the cells are mostly lysed and gutted. These findings, in agreement with EPR evidence, suggest the possibility that the antimicrobial activity of N-19004 might be linked to a membranolytic mechanism, potentially involving pore formation,[54–56] which could subsequently lead to cytoplasmic leakage.

DISCUSSION

The emergence and proliferation of drug-resistant bacterial infections stand as a critical global health challenge. This issue is particularly relevant in conditions such as cystic fibrosis, where persistent bacterial colonization and the succeeding, unregulated immune activation exacerbate disease progression. In this study, we have reported the chemical synthesis and *in vitro* and *in vivo* evaluation of a mini-library of amphiphilic compounds **1–6**, conceived to investigate their potential bifunctional pharmacological properties as antimicrobial and anti-inflammatory agents. These efforts represent an extension of our previous work on N-19004,[19] an anti-inflammatory small molecule designed as the FPR1 antagonist and herein repurposed as an antibacterial agent. The synthetic approach to compounds **1–6** was devised, exploring two distinct methodologies, with the aim of determining the most efficient route for subsequent large-scale production. The new approach, involving a reduced number of synthetic steps, demonstrated to be more efficient than the previous route, employed for the preparation of N-19004.[19] An extensive *in vitro* screening against a wide range of pathogens, including relevant clinical isolates and antibiotic-resistant bacterial strains such us MRSA and *Pseudomonas aeruginosa* RP73, revealed that all compounds exhibited interesting antibacterial properties regardless the structural differences between Gram-negative and Gram-positive bacterial membranes. It should be noted that while the ideal MIC range for clinical candidates generally falls between 1 and 10 μM, compound N-19004 was not selected solely based on its *in vitro* potency. Rather, its advancement was supported by a favorable overall profile, including drug-likeness, chemical stability, and proven efficacy in previous *in vivo* models.

A closer look at the MIC values (Table 1) in relation to the structural variations of **1-6** reveals that N-19004 displayed the highest efficacy against both Gram-positive and Gram-negative strains. The structural N-19004 congener, i.e., its sulfoxide derivative, N-19004-S, also demonstrated an intriguing activity profile and was therefore also chosen for subsequent *in vitro* studies.

A comparative study with previously reported arylamide foldamers[26,27] revealed that both N-19004 and its congener N-19004-S have lower efficacy *in vitro* against both Gram-positive and Gram-negative strains. It is worth noting that, unlike previously reported compounds, our molecules have a monomeric structure. This difference in molecular architecture may partially account for the reduced antibacterial potency, as foldamers often benefit from defined 3D conformations that can enhance target binding or membrane interaction. The simpler monomeric nature of our compound may also contribute to its lower hemolytic toxicity,[26,27] which suggests a potentially improved therapeutic window for N-19004.

Preliminary structure-activity relationship (SAR) studies revealed a crucial role of the 2-naphthylmethyl moiety for the antibacterial activity, as its replacement with a phenethyl (as in **3**), benzyl (as in **4**), or even 1-naphthylmethyl (as in **5**) reduced the antibacterial efficacy, especially against Gram-negative strains. Similarly, polar heads preorganization[19] dictated by the β-alanine linkers in compounds **1** and **3** markedly affected the antibacterial potential, as β-alanine replacement with the longer γ-aminobutyric acid (leading to compound **6**) resulted in a measurable drop in the activity against almost all the tested strains.

Subsequent crystal violet assays and CLSM analyses, performed on compounds **1** and **2**, demonstrated that they significantly inhibited biofilm formation in MDR *Pseudomonas aeruginosa* and *Staphylococcus aureus* strains. When tested on preformed biofilms, N-19004 induced substantial alterations in the biofilm architecture of *Pseudomonas aeruginosa* and *Staphylococcus aureus* strains, along with a deep reduction of their biofilm biovolume. Recent similar studies have shown that compounds capable of perturbing membrane integrity can also interfere with quorum sensing and the production of extracellular

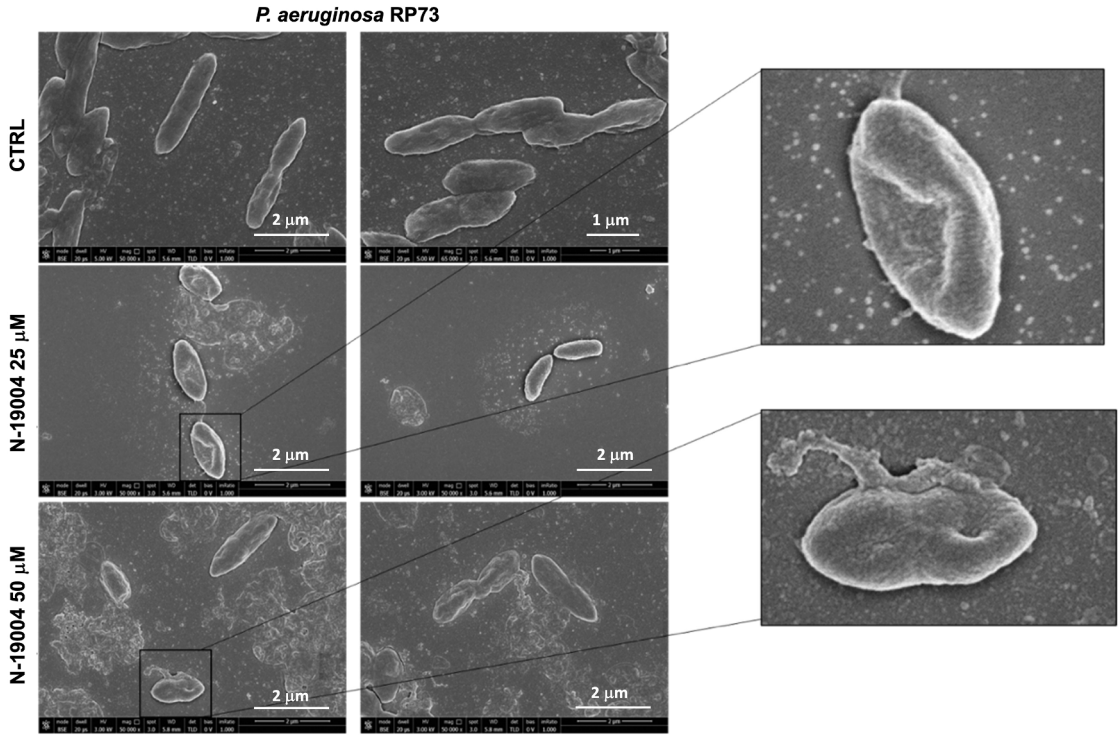

Figure 9. Scanning electron microscopy (SEM) images of *Pseudomonas aeruginosa* RP73 bacterial cells upon treatment with N-19004

Cells are analyzed upon treatment with N-19004 for 16h. Bars: 1 or 2 μm.

polymeric substances (EPS), both of which are critical for biofilm development and stability.[56] In a pre-clinical mouse model of chronic lung infection caused by *Pseudomonas aeruginosa* MDR-RP73, N-19004 (as the most promising candidate) displayed excellent anti-microbial and anti-inflammatory efficacy. Different from most anti-bacterial/anti-inflammatory agents reported to date,[16,17] our experimental data indicated that these two pharmacological activities were most likely independent of each other. N-19004 achieves complete bacterial eradication at low concentrations, whereas its anti-inflammatory effect becomes apparent only at slightly higher doses, after the pathogen load has already been cleared.

From a mechanistic standpoint, EPR spectroscopy and SEM analyses suggest that N-19004 acts as an antibacterial agent via a membranolytic action, involving pore formation and subsequent cytoplasmic leakage. This behavior closely resembles that of cationic antimicrobial peptides (CAMPs), which are well-documented for their ability to target bacterial membranes.[49] However, in contrast to CAMPs, N-19004 possesses a significantly smaller molecular structure. While this feature allows overcoming several limitations associated with CAMPs, including the susceptibility to proteolytic degradation,[57,58] the reduced molecular size does not align with its capacity to disrupt bacterial membranes, although this property is not unique among antimicrobial compounds[59] and ''short-chain'' peptides.[60] Efforts involving both experimental and computational studies[60] will be conducted to provide in-depth mechanistic insights, enabling to the clarification of the role of N-19004 in bacterial membrane disruption. Likewise, based on previous evidence,[19] the *in vivo* anti-inflammatory properties of N-19004 have been attributed to its antagonistic activity against FPR-1. While it is established that FPR-1 activation plays a key role in innate immune response against bacterial infections,[61] its specific contribution to the inflammatory processes triggered by *Pseudomonas aeruginosa* remains to be clearly defined.[62] Accordingly, future studies will be aimed at unraveling the role of FPR-1 in *Pseudomonas aeruginosa*-induced inflammation and to assess whether the pharmacological properties of N-19004 derive from targeting this pathway.

Overall, given the combined antimicrobial and anti-inflammatory activity, N-19004 represents a convenient alternative to current therapeutic strategies targeting chronic infections. To date, very few compounds have been reported to target both bacterial persistence and chronic inflammation simultaneously.[13,14] Because of its small size and minimal molecular structure, chemical synthesis of N-19004 is more cost-effective and scalable than the majority of the synthetic protocols devised for the preparation of current clinical and preclinical candidates. Additionally, the low molecular weight allows the use of low doses *in vivo*, on a mg/Kg basis. The pharmacological properties of N-19004 extend beyond those already reported in the animal model of age-related macular degeneration (AMD),[19] which demonstrated the ability of this molecule to inhibit angiogenic/inflammatory processes commonly associated with this pathology. This highlights the versatile and

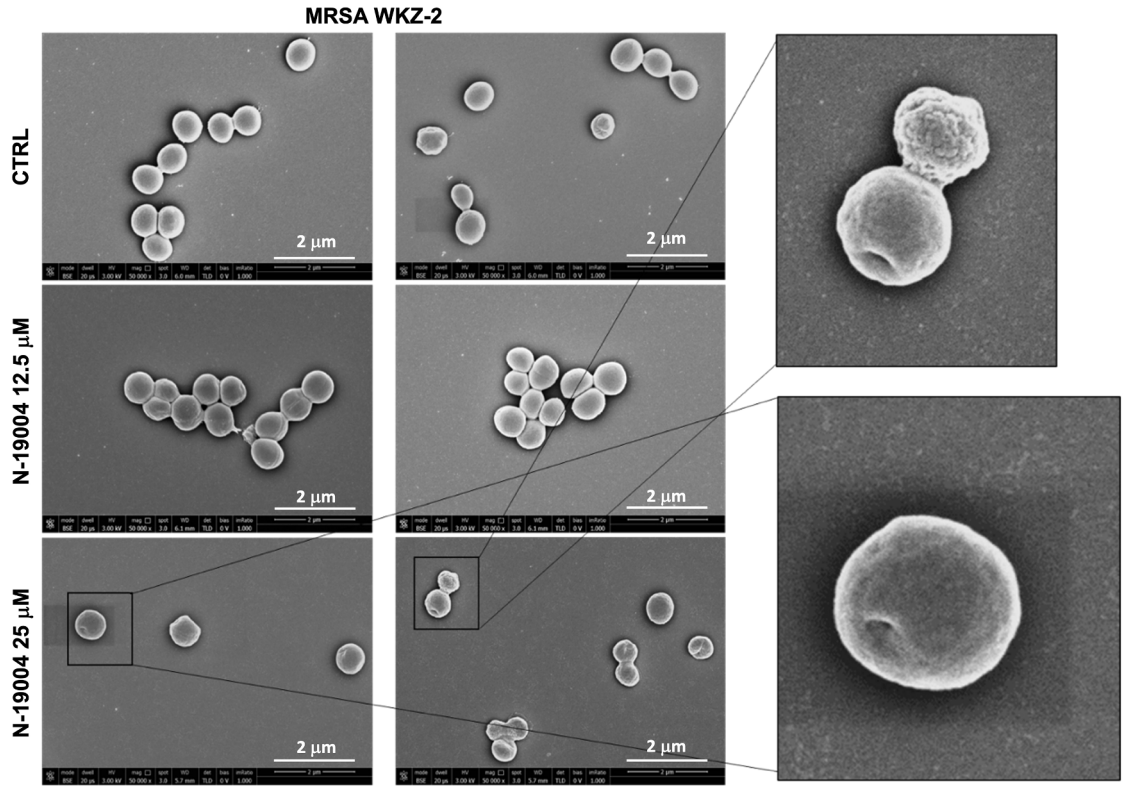

Figure 10. Scanning electron microscopy (SEM) images of *Staphylococcus aureus* MRSA WKZ-2 bacterial cells upon treatment with N-19004
Cells are analyzed upon treatment with N-19004 for 16h. Bars: 2 μm.

promising pharmacological potential of N-19004, encouraging its further preclinical development.

Limitations of the study

Despite the substantial amount of data presented in this article, several limitations must be recognized. First, while *in vitro* studies have been primarily focused on the antibacterial activity of N-19004 and its derivatives against *Staphylococcus aureus* and *Pseudomonas aeruginosa* (as representative examples of Gram-positive and Gram-negative pathogens), our *in vivo* investigations have been limited to *Pseudomonas aeruginosa*-infected mice. This highlights the need for the future validation of the antibacterial effect of N-19004 against *S. aureus* in animal models.

Additionally, most of our *in vivo* data are derived from the use of C57Bl/6NCrlBR mice infected with *Pseudomonas aeruginosa* RP73 (as an example of MDR strains). Even though this model is widely employed for a preliminary assessment of the antibacterial/anti-inflammatory efficacy in CF lung infection models, future studies will need to incorporate other animal models, including CFTR knockout mice, to more accurately reproduce the pathophysiological features of CF in humans.

Eventually, the mechanism ruling the antibacterial effect of N-19004 remains not fully elucidated in this study. While EPR and SEM analyses have suggested a mode of action involving the disruption of the bacterial membrane bilayer. The quantification of extracellular DNA release by UV-vis measurements and determination of changes in K^+ in the medium by flame photometry would be helpful to gain deeper membranolytic mechanistic insight. Also, further studies are required to highlight whether additional pathways, such as intracellular target interference or oxidative stress induction, may have a role in the overall bactericidal activity.

RESOURCE AVAILABILITY

Lead contact

Further information and requests for resources and reagents should be directed to and will be fulfilled by the lead contact, Daniele D'Alonzo (dandalonzo@unina.it).

Materials availability

The peptidomimetics synthesized in this study are available from the lead contact upon request.

Data and code availability

Data have been deposited at the Harvard Dataverse repository and are publicly available as of the date of publication. Accession numbers are listed in the key resources table.

ACKNOWLEDGMENTS

M.D.F. is grateful to the Italian MUR for being granted a research fellow position (PONR&I 2014–2020, CUP E65F21003010003). Financial support from Campania Region, Scientific Research Department, POR-FESR 2014–2020, Grant B61C17000070007 (OR3) and from European Union, "Fondo Europeo di Sviluppo Regionale," project "Contratto di sviluppo CDS 000463 - Altergon Italia Srl," PON Imprese e Competitività 2014–2020, Grant C68I15000180008,

to V.P. is kindly acknowledged for this study. Part of the authors' work described in this article was supported by Italian MUR, PRIN 2020, Project SEA-WAVE 2020BKK3W9 (CUP E69J22001140005). The authors finally acknowledge the Italian MUR program "Dipartimenti di Eccellenza 2023-2027" for the project "ArCHIMede" (CUP E63C22003710006).

AUTHOR CONTRIBUTIONS

Conceptualization, D.D. and V.P.; methodology, D.D., A.A., G.D.E., and A.B.; investigation, M.D.F, R.G., M.C., A.R., M.C., A.C., D.G., and I.D.F.; writing-original draft, M.D.F., R.G., M.C., and A.R.; writing—review and editing, M.D.F., D.D., V.P., A.L., M.C., G.D.E., L.P., A.A., R.G., A.B., I.D.F., and D.G.; funding acquisition, V.P., A.L., and A.A.; supervision, D.D., V.P., A.A., A.B., and G.D.E.

DECLARATION OF INTERESTS

M.D.F., V.P., and D.D. are the founders of IRIDEA S.r.l. (https://irideapharma.com). IRIDEA is a university spin-off with a focus on the identification of small-molecule therapeutics with anti-angiogenic and anti-inflammatory properties. M.D.F., V.P., and D.D. are inventors of the patent application WO2023203473A1, assigned to IRIDEA S.r.l.

STAR★METHODS

Detailed methods are provided in the online version of this paper and include the following:

- KEY RESOURCES TABLE
- EXPERIMENTAL MODEL AND STUDY PARTICIPANT DETAILS
  - Mouse model
- METHOD DETAILS
  - Chemical synthesis
  - Synthesis of compound 3
  - Synthesis of compound 4
  - Synthesis of compound 5
  - Synthesis of compound 6
  - *In vitro* studies
  - *In vivo* experiments
  - EPR experiments on bacterial model membranes
- QUANTIFICATION AND STATISTICAL ANALYSIS
  - *In vitro* studies
  - *In vivo* studies

SUPPLEMENTAL INFORMATION

Supplemental information can be found online at https://doi.org/10.1016/j.isci.2025.113674.

Received: May 13, 2025
Revised: July 16, 2025
Accepted: September 29, 2025
Published: October 3, 2025

REFERENCES

1. Ho, C.S., Wong, C.T.H., Aung, T.T., Lakshminarayanan, R., Mehta, J.S., Rauz, S., McNally, A., Kintses, B., Peacock, S.J., De La Fuente-Nunez, C., et al. (2025). Antimicrobial resistance: a concise update. Lancet Microbe *6*, 100947. https://doi.org/10.1016/j.lanmic.2024.07.010.
2. Naghavi, M., Vollset, S.E., Ikuta, K.S., Swetschinski, L.R., Gray, A.P., Wool, E.E., Robles Aguilar, G., Mestrovic, T., Smith, G., Han, C., et al. (2024). Global burden of bacterial antimicrobial resistance 1990–2021: a systematic analysis with forecasts to 2050. Lancet *404*, 1199–1226. https://doi.org/10.1016/S0140-6736(24)01867-1.
3. Miller, W.R., and Arias, C.A. (2024). ESKAPE pathogens: antimicrobial resistance, epidemiology, clinical impact and therapeutics. Nat. Rev. Microbiol. *22*, 598–616. https://doi.org/10.1038/s41579-024-01054-w.
4. Tommasi, R., Brown, D.G., Walkup, G.K., Manchester, J.I., and Miller, A.A. (2015). ESKAPEing the labyrinth of antibacterial discovery. Nat. Rev. Drug Discov. *14*, 529–542. https://doi.org/10.1038/nrd4572.
5. Blair, J.M.A., Webber, M.A., Baylay, A.J., Ogbolu, D.O., and Piddock, L.J.V. (2015). Molecular mechanisms of antibiotic resistance. Nat. Rev. Microbiol. *13*, 42–51. https://doi.org/10.1038/nrmicro3380.
6. Horne, M., Woolley, I., and Lau, J.S.Y. (2024). The Use of Long-term Antibiotics for Suppression of Bacterial Infections. Clin. Infect. Dis. *79*, 848–854. https://doi.org/10.1093/cid/ciae302.
7. Hancock, R.E.W., and Speert, D.P. (2000). Antibiotic resistance in *Pseudomonas aeruginosa*: mechanisms and impact on treatment. Drug Resist. Updat. *3*, 247–255. https://doi.org/10.1054/drup.2000.0152.
8. Turner, N.A., Sharma-Kuinkel, B.K., Maskarinec, S.A., Eichenberger, E.M., Shah, P.P., Carugati, M., Holland, T.L., and Fowler, V.G. (2019). Methicillin-resistant Staphylococcus aureus: an overview of basic and clinical research. Nat. Rev. Microbiol. *17*, 203–218. https://doi.org/10.1038/s41579-018-0147-4.
9. Cohen-Cymberknoh, M. (2024). Infection and Inflammation in the Cystic fibrosis (CF) airway. Pediatr. Pulmonol. *60 Suppl 1*, S82–S83. https://doi.org/10.1002/ppul.27355.
10. LiPuma, J.J. (2010). The Changing Microbial Epidemiology in Cystic Fibrosis. Clin. Microbiol. Rev. *23*, 299–323. https://doi.org/10.1128/CMR.00068-09.
11. (2023). Cystic Fibrosis Foundation Patient Registry. Annual Data Report. https://www.cff.org/medical-professionals/patient-registry.
12. Chmiel, J.F., and Davis, P.B. (2003). State of the Art: Why do the lungs of patients with cystic fibrosis become infected and why can't they clear the infection? Respir. Res. *4*, 8. https://doi.org/10.1186/1465-9921-4-8.
13. Sheikh, Z., Bradbury, P., Reekie, T.A., Pozzoli, M., Robinson, P.D., Kassiou, M., Young, P.M., Ong, H.X., and Traini, D. (2021). Tobramycin and Colistin display anti-inflammatory properties in CuFi-1 cystic fibrosis cell line. Eur. J. Pharmacol. *902*, 174098. https://doi.org/10.1016/j.ejphar.2021.174098.
14. Venditto, V.J., Haydar, D., Abdel-Latif, A., Gensel, J.C., Anstead, M.I., Pitts, M.G., Creameans, J., Kopper, T.J., Peng, C., and Feola, D.J. (2021). Immunomodulatory Effects of Azithromycin Revisited: Potential Applications to COVID-19. Front. Immunol. *12*, 574425. https://doi.org/10.3389/fimmu.2021.574425.
15. Chen, L., Cheng, M., Song, K., Tian, X., Wong, A., Yang, Y., Wang, T., Tan, G.Y.A., and Choo, S.W. (2025). Harnessing traditional medicine: A dual-action antimicrobial combination against pathogens. iScience *28*, 111910. https://doi.org/10.1016/j.isci.2025.111910.
16. Zusso, M., Lunardi, V., Franceschini, D., Pagetta, A., Lo, R., Stifani, S., Frigo, A.C., Giusti, P., and Moro, S. (2019). Ciprofloxacin and levofloxacin attenuate microglia inflammatory response via TLR4/NF-kB pathway. J. Neuroinflammation *16*, 148. https://doi.org/10.1186/s12974-019-1538-9.
17. Gillan, J.L., Davidson, D.J., and Gray, R.D. (2021). Targeting cystic fibrosis inflammation in the age of CFTR modulators: focus on macrophages. Eur. Respir. J. *57*, 2003502. https://doi.org/10.1183/13993003.03502-2020.
18. Drevinek, P., Canton, R., Johansen, H.K., Hoffman, L., Coenye, T., Burgel, P.-R., and Davies, J.C. (2022). New concepts in antimicrobial resistance in cystic fibrosis respiratory infections. J. Cyst. Fibros. *21*, 937–945. https://doi.org/10.1016/j.jcf.2022.10.005.
19. De Fenza, M., Locri, F., Plastino, F., Chino, M., Maglio, O., Leone, L., Gazzaroli, G., Belleri, M., Giacomini, A., Kvanta, A., et al. (2024). Turn-Adopting Peptidomimetic as a Formyl Peptide Receptor-1 Antagonist. ACS Pharmacol. Transl. Sci. *7*, 3476–3487. https://doi.org/10.1021/acsptsci.4c00366.

20. Weiß, E., and Kretschmer, D. (2018). Formyl-Peptide Receptors in Infection, Inflammation, and Cancer. Trends Immunol. *39*, 815–829. https://doi.org/10.1016/j.it.2018.08.005.

21. Ahmet, D.S., Basheer, H.A., Salem, A., Lu, D., Aghamohammadi, A., Weyerhäuser, P., Bordiga, A., Almeniawi, J., Rashid, S., Cooper, P.A., et al. (2020). Application of small molecule FPR1 antagonists in the treatment of cancers. Sci. Rep. *10*, 17249. https://doi.org/10.1038/s41598-020-74350-z.

22. Cammalleri, M., Dal Monte, M., Pavone, V., De Rosa, M., Rusciano, D., and Bagnoli, P. (2019). The uPAR System as a Potential Therapeutic Target in the Diseased Eye. Cells *8*, 925. https://doi.org/10.3390/cells8080925.

23. D'Alonzo, D., De Fenza, M., and Pavone, V. (2020). COVID-19 and pneumonia: a role for the uPA/uPAR system. Drug Discov. Today *25*, 1528–1534. https://doi.org/10.1016/j.drudis.2020.06.013.

24. He, S., and Deber, C.M. (2024). Interaction of designed cationic antimicrobial peptides with the outer membrane of gram-negative bacteria. Sci. Rep. *14*, 1894. https://doi.org/10.1038/s41598-024-51716-1.

25. Fjell, C.D., Hiss, J.A., Hancock, R.E.W., and Schneider, G. (2011). Designing antimicrobial peptides: form follows function. Nat. Rev. Drug Discov. *11*, 37–51. https://doi.org/10.1038/nrd3591.

26. Tew, G.N., Scott, R.W., Klein, M.L., and DeGrado, W.F. (2010). De Novo Design of Antimicrobial Polymers, Foldamers, and Small Molecules: From Discovery to Practical Applications. Acc. Chem. Res. *43*, 30–39. https://doi.org/10.1021/ar900036b.

27. Choi, S., Isaacs, A., Clements, D., Liu, D., Kim, H., Scott, R.W., Winkler, J.D., and DeGrado, W.F. (2009). *De novo* design and *in vivo* activity of conformationally restrained antimicrobial arylamide foldamers. Proc. Natl. Acad. Sci. USA *106*, 6968–6973. https://doi.org/10.1073/pnas.0811818106.

28. Hanelt, S., Friedrich, J.F., Orts-Gil, G., and Meyer-Plath, A. (2012). Study of Lewis acid catalyzed chemical bromination and bromoalkylation of multi-walled carbon nanotubes. Carbon *50*, 1373–1385. https://doi.org/10.1016/j.carbon.2011.11.009.

29. Hanelt, S., Friedrich, J.F., and Meyer-Plath, A. (2013). UV Spectrometric Indirect Analysis of Brominated MWCNTs with UV Active Thiols and an Alkene—Reaction Kinetics, Quantification and Differentiation of Adsorbed Bromine and Oxygen. Materials *6*, 3035–3063. https://doi.org/10.3390/ma6083035.

30. La Gatta, S., Leone, L., Maglio, O., De Fenza, M., Nastri, F., Pavone, V., Chino, M., and Lombardi, A. (2021). Unravelling the Structure of the Tetrahedral Metal-Binding Site in METP3 through an Experimental and Computational Approach. Molecules *26*, 5221. https://doi.org/10.3390/molecules26175221.

31. Chino, M., La Gatta, S., Leone, L., De Fenza, M., Lombardi, A., Pavone, V., and Maglio, O. (2023). Dye Decolorization by a Miniaturized Peroxidase Fe-MimochromeVI*a. Int. J. Mol. Sci. *24*, 11070. https://doi.org/10.3390/ijms241311070.

32. Sanguinetti, M., Sanfilippo, S., Castagnolo, D., Sanglard, D., Posteraro, B., Donzellini, G., and Botta, M. (2013). Novel Macrocyclic Amidinoureas: Potent Non-Azole Antifungals Active against Wild-Type and Resistant Candida Species. ACS Med. Chem. Lett. *4*, 852–857. https://doi.org/10.1021/ml400187w.

33. Thomas, J.B., Atkinson, R.N., Namdev, N., Rothman, R.B., Gigstad, K.M., Fix, S.E., Mascarella, S.W., Burgess, J.P., Vinson, N.A., Xu, H., et al. (2002). Discovery of an Opioid κ Receptor Selective Pure Antagonist from a Library of N-Substituted 4β-Methyl-5-(3-hydroxyphenyl)morphans. J. Med. Chem. *45*, 3524–3530. https://doi.org/10.1021/jm020084h.

34. Gaglione, R., Dell'Olmo, E., Bosso, A., Chino, M., Pane, K., Ascione, F., Itri, F., Caserta, S., Amoresano, A., Lombardi, A., et al. (2017). Novel human bioactive peptides identified in Apolipoprotein B: Evaluation of their therapeutic potential. Biochem. Pharmacol. *130*, 34–50. https://doi.org/10.1016/j.bcp.2017.01.009.

35. Dell'Olmo, E., Gaglione, R., Sabbah, M., Schibeci, M., Cesaro, A., Di Girolamo, R., Porta, R., and Arciello, A. (2021). Host defense peptides identified in human apolipoprotein B as novel food biopreservatives and active coating components. Food Microbiol. *99*, 103804. https://doi.org/10.1016/j.fm.2021.103804.

36. Cesaro, A., Torres, M.D.T., Gaglione, R., Dell'Olmo, E., Di Girolamo, R., Bosso, A., Pizzo, E., Haagsman, H.P., Veldhuizen, E.J.A., De La Fuente-Nunez, C., and Arciello, A. (2022). Synthetic Antibiotic Derived from Sequences Encrypted in a Protein from Human Plasma. ACS Nano *16*, 1880–1895. https://doi.org/10.1021/acsnano.1c04496.

37. Gaglione, R., Smaldone, G., Cesaro, A., Rumolo, M., De Luca, M., Di Girolamo, R., Petraccone, L., Del Vecchio, P., Oliva, R., Notomista, E., et al. (2021). Impact of a Single Point Mutation on the Antimicrobial and Fibrillogenic Properties of Cryptides from Human Apolipoprotein B. Pharmaceuticals *14*, 631. https://doi.org/10.3390/ph14070631.

38. Cesaro, A., Gaglione, R., Chino, M., De Luca, M., Di Girolamo, R., Lombardi, A., Filosa, R., and Arciello, A. (2022). Novel Retro-Inverso Peptide Antibiotic Efficiently Released by a Responsive Hydrogel-Based System. Biomedicines *10*, 1301. https://doi.org/10.3390/biomedicines10061301.

39. Falagas, M.E., Vouloumanou, E.K., Samonis, G., and Vardakas, K.Z. (2016). Fosfomycin. Clin. Microbiol. Rev. *29*, 321–347. https://doi.org/10.1128/CMR.00068-15.

40. Silva, V., Almeida, L., Gaio, V., Cerca, N., Manageiro, V., Caniça, M., Capelo, J.L., Igrejas, G., and Poeta, P. (2021). Biofilm Formation of Multidrug-Resistant MRSA Strains Isolated from Different Types of Human Infections. Pathogens *10*, 970. https://doi.org/10.3390/pathogens10080970.

41. Kunz Coyne, A.J., El Ghali, A., Holger, D., Rebold, N., and Rybak, M.J. (2022). Therapeutic Strategies for Emerging Multidrug-Resistant *Pseudomonas aeruginosa*. Infect. Dis. Ther. *11*, 661–682. https://doi.org/10.1007/s40121-022-00591-2.

42. Cigana, C., Lorè, N.I., Riva, C., De Fino, I., Spagnuolo, L., Sipione, B., Rossi, G., Nonis, A., Cabrini, G., and Bragonzi, A. (2016). Tracking the immunopathological response to *Pseudomonas aeruginosa* during respiratory infections. Sci. Rep. *6*, 21465. https://doi.org/10.1038/srep21465.

43. Cigana, C., Ranucci, S., Rossi, A., De Fino, I., Melessike, M., and Bragonzi, A. (2020). Antibiotic efficacy varies based on the infection model and treatment regimen for *Pseudomonas aeruginosa*. Eur. Respir. J. *55*, 1802456. https://doi.org/10.1183/13993003.02456-2018.

44. A. Filloux, J.-L. Ramos, and Springer Science+Business Media., eds. (2014). *Pseudomonas*: methods and protocols (Humana Press).

45. Facchini, M., De Fino, I., Riva, C., and Bragonzi, A. (2014). Long Term Chronic *Pseudomonas aeruginosa* Airway Infection in Mice. J. Vis. Exp. *51019*. https://doi.org/10.3791/51019-v.

46. Bragonzi, A. (2010). Murine models of acute and chronic lung infection with cystic fibrosis pathogens. Int. J. Med. Microbiol. *300*, 584–593. https://doi.org/10.1016/j.ijmm.2010.08.012.

47. Kukavica-Ibrulj, I., Facchini, M., Cigana, C., Levesque, R.C., and Bragonzi, A. (2014). Assessing *Pseudomonas aeruginosa* Virulence and the Host Response Using Murine Models of Acute and Chronic Lung Infection. In *Pseudomonas*: Methods and Protocols Methods in Molecular Biology, A. Filloux and J.-L. Ramos, eds. (New York: Springer), pp. 757–771. https://doi.org/10.1007/978-1-4939-0473-0_58.

48. Bianconi, I., Jeukens, J., Freschi, L., Alcalá-Franco, B., Facchini, M., Boyle, B., Molinaro, A., Kukavica-Ibrulj, I., Tümmler, B., Levesque, R.C., and Bragonzi, A. (2015). Comparative genomics and biological characterization of sequential *Pseudomonas aeruginosa* isolates from persistent airways infection. BMC Genom. *16*, 1105. https://doi.org/10.1186/s12864-015-2276-8.

49. Chen, E.H.-L., Wang, C.-H., Liao, Y.-T., Chan, F.-Y., Kanaoka, Y., Uchihashi, T., Kato, K., Lai, L., Chang, Y.-W., Ho, M.-C., and Chen, R.P.Y. (2023). Visualizing the membrane disruption action of antimicrobial peptides by cryo-electron tomography. Nat. Commun. *14*, 5464. https://doi.org/10.1038/s41467-023-41156-2.

50. Huan, Y., Kong, Q., Mou, H., and Yi, H. (2020). Antimicrobial Peptides: Classification, Design, Application and Research Progress in Multiple Fields. Front. Microbiol. *11*, 582779. https://doi.org/10.3389/fmicb.2020.582779.

51. Oliva, R., Chino, M., Pane, K., Pistorio, V., De Santis, A., Pizzo, E., D'Errico, G., Pavone, V., Lombardi, A., Del Vecchio, P., et al. (2018). Exploring the role of unnatural amino acids in antimicrobial peptides. Sci. Rep. *8*, 8888. https://doi.org/10.1038/s41598-018-27231-5.

52. Fischer, W. (1994). Lipoteichoic acid and lipids in the membrane of *Staphylococcus aureus*. Med. Microbiol. Immunol. *183*, 61–76. https://doi.org/10.1007/BF00277157.

53. Lam, J.S., Taylor, V.L., Islam, S.T., Hao, Y., and Kocíncová, D. (2011). Genetic and Functional Diversity of *Pseudomonas aeruginosa* Lipopolysaccharide. Front. Microbiol. *2*, 118. https://doi.org/10.3389/fmicb.2011.00118.

54. Gaglione, R., Cesaro, A., Dell'Olmo, E., Della Ventura, B., Casillo, A., Di Girolamo, R., Velotta, R., Notomista, E., Veldhuizen, E.J.A., Corsaro, M.M., et al. (2019). Effects of human antimicrobial cryptides identified in apolipoprotein B depend on specific features of bacterial strains. Sci. Rep. *9*, 6728. https://doi.org/10.1038/s41598-019-43063-3.

55. Hartmann, M., Berditsch, M., Hawecker, J., Ardakani, M.F., Gerthsen, D., and Ulrich, A.S. (2010). Damage of the Bacterial Cell Envelope by Antimicrobial Peptides Gramicidin S and PGLa as Revealed by Transmission and Scanning Electron Microscopy. Antimicrob. Agents Chemother. *54*, 3132–3142. https://doi.org/10.1128/AAC.00124-10.

56. Batoni, G., Maisetta, G., and Esin, S. (2016). Antimicrobial peptides and their interaction with biofilms of medically relevant bacteria. Biochim. Biophys. Acta *1858*, 1044–1060. https://doi.org/10.1016/j.bbamem.2015.10.013.

57. Lu, J., Xu, H., Xia, J., Ma, J., Xu, J., Li, Y., and Feng, J. (2020). D- and Unnatural Amino Acid Substituted Antimicrobial Peptides With Improved Proteolytic Resistance and Their Proteolytic Degradation Characteristics. Front. Microbiol. *11*, 563030. https://doi.org/10.3389/fmicb.2020.563030.

58. Lei, J., Sun, L., Huang, S., Zhu, C., Li, P., He, J., Mackey, V., Coy, D.H., and He, Q. (2019). The antimicrobial peptides and their potential clinical applications. Am. J. Transl. Res. *11*, 3919–3931.

59. De Gregorio, E., Esposito, A., Vollaro, A., De Fenza, M., D'Alonzo, D., Migliaccio, A., Iula, V.D., Zarrilli, R., and Guaragna, A. (2020). N-Nonyloxypentyl-L-Deoxynojirimycin Inhibits Growth, Biofilm Formation and Virulence Factors Expression of *Staphylococcus aureus*. Antibiotics *9*, 362. https://doi.org/10.3390/antibiotics9060362.

60. Koneru, J.K., Prakashchand, D.D., Dube, N., Ghosh, P., and Mondal, J. (2021). Spontaneous transmembrane pore formation by short-chain synthetic peptide. Biophys. J. *120*, 4557–4574. https://doi.org/10.1016/j.bpj.2021.08.033.

61. Migeotte, I., Communi, D., and Parmentier, M. (2006). Formyl peptide receptors: A promiscuous subfamily of G protein-coupled receptors controlling immune responses. Cytokine Growth Factor Rev. *17*, 501–519. https://doi.org/10.1016/j.cytogfr.2006.09.009.

62. Rada, B. (2017). Interactions between Neutrophils and *Pseudomonas aeruginosa* in Cystic Fibrosis. Pathogens *6*, 10. https://doi.org/10.3390/pathogens6010010.

63. Wiegand, I., Hilpert, K., and Hancock, R.E.W. (2008). Agar and broth dilution methods to determine the minimal inhibitory concentration (MIC) of antimicrobial substances. Nat. Protoc. *3*, 163–175. https://doi.org/10.1038/nprot.2007.521.

64. Ernst, R.K., Hajjar, A.M., Tsai, J.H., Moskowitz, S.M., Wilson, C.B., and Miller, S.I. (2003). *Pseudomonas aeruginosa* lipid A diversity and its recognition by Toll-like receptor 4. J. Endotoxin Res. *9*, 395–400. https://doi.org/10.1179/096805103225002764.

65. King, J.D., Kocíncová, D., Westman, E.L., and Lam, J.S. (2009). Review: Lipopolysaccharide biosynthesis in *Pseudomonas aeruginosa*. Innate Immun. *15*, 261–312. https://doi.org/10.1177/1753425909106436.

66. Bystrova, O.V., Knirel, Y.A., Lindner, B., Kocharova, N.A., Kondakova, A.N., Zähringer, U., and Pier, G.B. (2006). Structures of the core oligosaccharide and O-units in the R- and SR-type lipopolysaccharides of reference strains of *Pseudomonas aeruginosa* O-serogroups. FEMS Immunol. Med. Microbiol. *46*, 85–99. https://doi.org/10.1111/j.1574-695X.2005.00004.x.

67. Morath, S., Geyer, A., and Hartung, T. (2001). Structure–Function Relationship of Cytokine Induction by Lipoteichoic Acid from *Staphylococcus aureus*. J. Exp. Med. *193*, 393–397. https://doi.org/10.1084/jem.193.3.393.

68. Bharatiya, B., Wang, G., Rogers, S.E., Pedersen, J.S., Mann, S., and Briscoe, W.H. (2021). Mixed liposomes containing gram-positive bacteria lipids: Lipoteichoic acid (LTA) induced structural changes. Colloids Surf. B Biointerfaces *199*, 111551. https://doi.org/10.1016/j.colsurfb.2020.111551.

69. Galdiero, S., Falanga, A., Vitiello, G., Vitiello, M., Pedone, C., D'Errico, G., and Galdiero, M. (2010). Role of membranotropic sequences from herpes simplex virus type I glycoproteins B and H in the fusion process. Biochim. Biophys. Acta *1798*, 579–591. https://doi.org/10.1016/j.bbamem.2010.01.006.

STAR★METHODS

KEY RESOURCES TABLE

REAGENT or RESOURCE	SOURCE	IDENTIFIER
Bacterial and virus strains		
Burkholderia cenocepacia	Clinical isolate	*LMG 18863*
Burkholderia multivorans	Clinical isolate	*LMG 17582*
Burkholderia cenocepacia	Clinical isolate	*J2315*
Pseudomonas aeruginosa AA2	Clinical Isolate	LMG27630
Pseudomonas aeruginosa	Clinical isolate	PAO1
Pseudomonas aeruginosa	Clinical isolate	KK27
Pseudomonas aeruginosa	The strain was a clinical isolate kindly provided by the Italian Cystic Fibrosis Research Foundation (FFC)	RP73
Enterococcus faecalis	American Type Culture Collection	29212
Straphylococcus aureus	American Type Culture Collection	12600
Straphylococcus aureus	American Type Culture Collection	29213
Straphylococcus aureus MRSA	The strain was a clinical isolate kindly provided by the Italian Cystic Fibrosis Research Foundation (FFC)	*(WKZ-2)*
Salmonella enterica serovar Typhimurium	American Type Culture Collection	14028
Acinetobacter baumannii	American Type Culture Collection	19606
Chemicals, peptides, and recombinant proteins		
2-phenylethanethiol	Merck	252581 (Sigma Aldrich)
2,6-dinitro-4-*t*-butyl-phenol	Carbosynth	FB70092
Boc-β-alanine	Merck	15382 (Sigma Aldrich)
1H-pirazole-1-carboxyamidine hydrochloride	Merck	402516 (Sigma Aldrich)
Phenylmethanethiol	Merck	B25401 (Sigma Aldrich)
3-Aminopropionic acid	Merck	05160 (Sigma Aldrich)
N,N′-Di-Boc-*1H*-pyrazole-1-carboxamidine	Merck	434167 (Sigma Aldrich)
1-Chlorometyl-naphtalene	Merck	25170 (Sigma Aldrich)
Thiourea	Merck	T8656 (Sigma Aldrich)
4-Aminobutyric acid	Merck	8.00302
1-palmitoyl-2-oleoyl-glycero-3-phosphocholine (POPC)	Avanti Research	850457
1-palmitoyl-2-oleoyl-sn-glycero-3-phospho-(1′-rac-glycerol) (sodium salt) (POPG)	Avanti Research	840457
1-palmitoyl-2-stearoyl-(5-doxyl)-sn-glycero-3-phosphocholine	Avanti Research	810601
1-palmitoyl-2-stearoyl-(7-doxyl)-sn-glycero-3-phosphocholine	Avanti Research	810602
1-palmitoyl-2-stearoyl-(10-doxyl)-sn-glycero-3-phosphocholine	Avanti Research	810603
1-palmitoyl-2-stearoyl-(14-doxyl)-sn-glycero-3-phosphocholine	Avanti Research	810605
Lipopolysaccharide (LPS) from *Pseudomonas aeruginosa*	Merck	L9143

(*Continued on next page*)

Continued		
REAGENT or RESOURCE	SOURCE	IDENTIFIER
Lipoteichoic acid (LTA) from *Staphylococcus aureus*	Merck	L2515
Critical commercial assays		
LIVE/DEAD® Bacterial Viability kit	Invitrogen	L7012 (ThermoFisher Scientific)
Experimental models: Cell lines		
Human red blood cells (RBCs)	Rockland	R405-0050
Experimental models: Organisms/strains		
Male mice	Charles River	RRID:IMSR_CRL:027
Software and algorithms		
GraphPad Prism (v9.5.1)	GraphPad Software	GraphPad Prism (RRID:SCR_002798)
MestreNova (v16.0.0)	MestreLab Research	https://mestrelab.com/
Origin (2018)	OriginLab	Origin (RRID:SCR_014212)
ChemDraw Professional (v16.0)	PerkinElmer	Chemdraw (RRID:SCR_016768)
Deposited data		
Repository	Harvard Dataverse	https://doi.org/10.7910/DVN/4ZB3G1.

EXPERIMENTAL MODEL AND STUDY PARTICIPANT DETAILS

Mouse model

Animal studies were conducted according to protocols approved by the San Raffaele Scientific Institute (Milan, Italy) Institutional Animal Care and Use Committee (IACUC # 1180) and adhered strictly to the Italian Ministry of Health guidelines for the use and care of experimental animals. Research with the *Pseudomonas aeruginosa* multidrug-resistant (MDR)-RP73 isolate from a CF individual and storage of biological materials were approved by the Ethics Commission of Hannover Medical School, Germany.

METHOD DETAILS

Chemical synthesis

All chemicals and solvents were purchased with the highest degree of purity (Merck, Alfa Aesar, VWR, Acros Organics, Romil) and used without further purification. The reactions were monitored by Thin Layer Chromatography (precoated silica gel plate F254, Merck) and the products were detected by exposure to UV source (254 nm) and iodine vapor. When possible, the reactions were also monitored by LC-MS analysis. Automated column chromatography separations in either direct or reverse phases were conducted with a Biotage Isolera chromatograph. HPLC analyses were performed on a Shimadzu LC-20ADxr equipped with an SPDM20A diode-array detector. HRMS spectra were recorded on a Shimadzu LCMS-IT-TOF system with ESI interface and Shimadzu LC-MS solution Workstation software for the data. NMR experiments were performed on spectrometers operating at 400 MHz (Bruker Avance), 500 MHz (Varian Inova) or 600 MHz (Bruker NEO Avance, equipped with triple resonance cryo-probe), all located at the Department of Chemical Sciences, University of Naples Federico II. NMR spectra of the synthetic intermediates were acquired using $CDCl_3$ solutions, unless otherwise specified. All spectra were analyzed and processed using MestreNova (MNova 15.0.1). The same software has been used to prepare the NMR figures presented in the ESI.

Synthesis of compound 3

(Phenethylthio)-4-(tert-butyl)-2,6-dinitrobenzene (9)

Compound **8**[19] (30.0 g, 0.076 mol), 2-phenylethanethiol (10.0 g, 0.072 mol, 0.95 eq.) and *N*,*N*-diisopropylethylamine (DIEA; 0.013 L, 0.076 mol, 1.0 eq.) were dissolved in anhydrous dichloromethane (DCM; 0.480 L). The solution was stirred under nitrogen atmosphere for 16 h. Afterwards, the solution was washed with 10% citric acid solution and then with a saturated sodium chloride (NaCl) solution. The organic phase was dried over sodium sulfate (Na_2SO_4). The crude was purified over silica gel (150 g; eluents: hexane and ethyl acetate, from 100:0 to 96:4), obtaining 25.1 g of thioether **9** (yield: 91.6 %). ^{1}H NMR (600 MHz, $CDCl_3$), δ: 1.37 (*s*, 9H), 2.87 (*t*, J = 8.2 Hz, 2H), 3.17 (*t*, J = 7.7 Hz, 2H), 7.15 (*d*, J = 7.3 Hz, 2H), 7.19 (*t*, J = 7.5 Hz, 1H), 7.27 (*t*, J= 7.4 Hz, 2H), 7.79 (*s*, 2H). ^{13}C NMR (150 MHz, $CDCl_3$), ppm: 30.8, 35.8, 36.0, 38.3, 100.1, 120.0, 123.7, 126.6, 128.6, 128.7, 139.1, 155.4. HRMS: calcd 361.114 ($[M\text{-}H]^+$); found 399.202 ($[M\text{-}K]^+$).

(Phenethylthio)-4-(tert-butyl)-2,6-diaminobenzene (10)

Compound **9** (10.0 g, 0.028 mol), ammonium chloride (7.9 g, 0.147 mol, 5.3 eq.) and zinc in powder (13.8 g, 0.211 mol, 7.6 eq.) were suspended in methanol (MeOH; 0.360 L) at 25.0 °C. The mixture was left under stirring in the dark and under argon atmosphere for

16h. The reaction mixture was evaporated and then filtered on a celite pad washing with toluene: 50:50. The filtrate was concentrated in vacuo affording **10** as a white-pink solid (8.56 g, >99%). ^{1}H NMR (400 MHz, DMSO-d_6), δ: 1.18 (*s*, 9H), 2.78 (*s*, 4H), 5.05 (*bs*, 4H), 6.06 (*s*, 2H), 7.16-7.20 (*m*, 3H), 7.26-7.30 (*m*, 5H). ^{13}C NMR (100 MHz, DMSO-d_6), ppm: 31.0, 34.0, 34.1, 35.5, 96.6, 100.0, 126.1, 128.2, 128.3, 140.5, 150.3, 152.4. HRMS: calcd 301.166 ([M-H]$^+$); found 301.088.

Di-tert-butyl (((5-(tert-butyl)-2-(phenethylthio)-1,3-phenylene)bis(azanediyl))bis(3-oxopropane-3,1-diyl))dicarbamate (11)

Boc-β-alanine (7.57 g, 0.04 mol, 2.0 eq.) was dissolved in anhydrous tetrahydrofuran (THF; 0.3 L) and cooled to -78°C under nitrogen atmosphere. Triethylamine (TEA; 0.018 L, 6.0 eq.) first and isobutylchloroformate (IBCF; 0.006 L, 0.048 mol, 2.4 eq.) then, were slowly added to the solution. The mixture was left while stirring for 1 h. After that, compound **10** (6.0 g, 0.02 mol) was dissolved in 0.175 L of anhydrous THF and added at the same temperature via a cannula. The reaction was left while stirring for 16h and slowly warmed to room temperature. The mixture was filtered and washed with ethyl acetate. The filtrate was concentrated under reduced pressure and the residue was purified over silica gel (150 g) using DCM:MeOH (from 100:0 to 98:2) as the eluent mixture, to obtain **11** as a reddish-brown oil (9.0 g, 70% yield). ^{1}H NMR (400 MHz, $CDCl_3$), δ: 1.45 (*s*, 9H), 1.54 (*s*, 18H), 2.58 (*t*, J = 8.0 Hz, 3H), 2.94 (*t*, J= 4.0 Hz, 3H), 3.01 (*t*, J = 8.0 Hz, 3H), 3.57 (*q*, J = 4.0 Hz, 3H),7.28 (*bs*, 2H), 7.35-7.38 (*m*, 2H), 7.42-7.46 (*m*, 3H), 8.38 (*bs*, 2H), 8.47 (*bs*, 2H). ^{13}C NMR (100 MHz, $CDCl_3$), ppm: 28.3, 30.8, 34.9, 36.0, 37.4, 79.4, 113.0, 127.0, 128.4, 128.8, 138.8, 140.0, 155.2, 156.0, 170.1. HRMS: calcd 643.345 ([M-H]$^+$); found 643.386.

N,N'-(5-(tert-butyl)-2-(phenethylthio)-1,3-phenylene)bis(3-guanidinopropanamide) (3)

Compound **11** (8.9 g, 0.014 mol) was suspended in trifluoroacetic acid (TFA; 0.090 L) at 0°C. The reaction was warmed to room temperature, left while stirring for 2 h and then dried *in vacuo*. The residue was dissolved in a water/acetonitrile (ACN) mixture (0.350 L, 1/1 v/v), then 1H-pirazole-1-carboxyamidine was added to the suspension (16.8 g, 0.152 mol, 10.0 eq). The resulting mixture was left while stirring for 16h at 25 °C. The solvent was removed under reduced pressure. The residue was purified by reverse-phase chromatography (RP-C18, eluents: water 0.1% TFA (v/v), acetonitrile 0.1% TFA (v/v)), obtaining 4.4 g of **3** as a white solid (60.3 % overall yield, TFA salt). ^{1}H NMR (400 MHz, D_2O), δ: 1.32 (*s*, 9H), 2.70-2.73 (*m*, 6H), 2.95 (*t*, J= 7.08 Hz, 2H), 3.55 (*t*, J = 6.13 Hz, 4H), 7.17 (*bd*, J =7.32 Hz, 2H), 7.28 (*bt*, J = 7.03 Hz, 1H), 7.34 (*t*, J = 7.05 Hz, 2H), 7.58 (*bs*, 2H). ^{13}C NMR (100 MHz, D_2O), ppm: 30.2, 34.4, 34.6, 35.2, 35.4, 37.4, 120.7, 126.4, 128.6, 128.7, 139.2, 139.7, 154.5, 156.4, 172.2. HRMS: calcd 527.283 ([M-H]$^+$); found 527.295.

Synthesis of compound 4

(Benzylthio)-4-(tert-butyl)-2,6-dinitrobenzene (12)

Compound **8**[19] (0.73 g, 1.85 mmol), benzylmercaptan (0.276 g, 2.22 mol, 1.2 eq.) and DIEA (0.322 mL, 1.85 mmol, 1.0 eq.) were dissolved in anhydrous DCM (12.0 mL). The solution was stirred under nitrogen atmosphere for 16 h. Afterwards, the solution was washed with 10% citric acid solution and then with a saturated NaCl solution. The organic phase was dried over sodium sulfate. The crude was purified over silica gel (30 g; eluents: hexane and ethyl acetate, from 100:0 to 70:30), obtaining 0.571 g of thioether **12** (yield: 88.9 %). ^{1}H NMR (600 MHz, $CDCl_3$), δ: 1.37 (*s*, 9H), 4.17 (*s*, 2H), 7.24-7.28 (*m*, 5H), 7.79 (*s*, 2H). ^{13}C NMR (150 MHz, $CDCl_3$), ppm: 30.8, 35.9, 42.4, 100.0, 118.9, 123.5, 128.2, 128.9, 129.5, 135.5, 156.0. HRMS: calcd 347.099 ([M-H]$^+$); found 386.189 ([M-K]$^+$).

(Benzylthio)-4-(tert-butyl)-2,6-diaminobenzene (14)

Compound **12** (0.550 g, 1.59 mmol), ammonium chloride (0.451 g, 8.43 mmol, 5.3 eq.) and zinc in powder (0.790 g, 12.1 mmol, 7.6 eq.) were suspended in methanol (20.0 mL) at 25.0 °C. The mixture was left under stirring in the dark and under argon atmosphere for 16h. The reaction mixture was evaporated and then filtered on a celite pad washing with toluene: 50:50. The filtrate was concentrated in vacuo affording **14** as a white-pink solid with a quantitative yield. ^{1}H NMR (600 MHz, CD_3CN), δ: 1.21 (*s*, 9H), 3.77 (*s*, 2H), 4.12 (*bs*, 4H), 6.24 (*s*, 2H), 7.23-7.29 (*m*, 5H). ^{13}C NMR (150 MHz, CD_3CN), ppm: 31.3, 35.1, 38.3, 103.5, 128.0, 129.4, 129.9, 139.4, 150.4, 155.0. HRMS: calcd 287.150 ([M-H]$^+$); found 287.135.

3-[N,N′-Bis(tert-butoxycarbonyl)guanidino]propionic acid

3-Aminopropionic acid (1.04 g, 11.7 mmol) was dissolved in a solvent mixture of ACN and water (102 mL; 8% v/v water). At 0 °C, DIEA (4.44 mL, 25.5 mmol) was added, followed by the gradual addition of *N,N′*-Di-Boc-*1H*-pyrazole-1-carboxamidine (2.90 g, 9.35 mmol). The reaction mixture was stirred at room temperature for 20 h. Upon completion, the reaction solvent was removed under reduced pressure. The crude product was redissolved in diethyl ether (Et_2O) and washed three times with 0.2 M acetic acid (AcOH). The combined organic layers were dried over sodium sulfate (Na_2SO_4) and subsequently concentrated under reduced pressure. This process afforded a white solid (3.09 g, 79.8 % yield). The product was characterized by ^{1}H and ^{13}C NMR spectroscopy, confirming its identity as the Boc-protected guanidino acid. The spectra were consistent with previously reported data in the literature.[32]

N,N'-(2-(benzylthio)-5-(tert-butyl)-1,3-phenylene)bis(3-guanidinopropanamide) (4)

Compound **14** (0.200 g, 0.699 mmol) was dissolved in anhydrous *N*,*N*-dimethylformamide (DMF; 0.015 L) under inert atmosphere. A mixture of 3-[*N*,*N′*-bis(*tert*-butoxycarbonyl)guanidino]propionic acid (0.500 g, 1.51 mmol, 2.2 eq.), hexafluorophosphate benzotriazole tetramethyl uranium (HBTU; 0.580 g, 1.51 mmol, 2.2 eq.), hydroxybenzotriazole (HOBt; 0.210 g, 1.51 mmol, 2.2 eq), DIEA (0.300 g, 2.32 mmol, 3.3 eq.) in anhydrous DMF (0.01 L) was added to the reaction flask via a cannula. The reaction mixture was stirred at room temperature for 2 hours. The reaction mixture was diluted with and washed with brine three times. The organic layers were collected, dried over Na_2SO_4 and evaporated under reduced pressure. The brownish crude was then treated with a mixture of TFA/TIS/H_2O (95:2.5:2.5; TIS = triisopropylsilane) at °0 C and left stirring for 2h at RT. The solvent was removed under reduced pressure. The residue was purified by diethyl ether precipitation first, and then by reverse-phase chromatography

(RP-C18, eluents: water 0.1% TFA (v/v), acetonitrile 0.1% TFA (v/v)), obtaining 0.247 g of **4** as a white solid (70 % yield, TFA salt). ^{1}H NMR (600 MHz, H_2O/D_2O= 90/10), δ: 1.22 (*s*, 9H), 2.59 (*t*, J = 13.0 Hz, 4H), 3.46 (*q*, J = 6.4 Hz, 4H), 3.67 (*s*, 2H), 6.89-6.90 (*m*, 2H), 7.14-7.16 (*m*, 3H), 7.20 (*bt*, 2H), 7.53 (*bs*, 2H), 9.25 (*bs*, 2H). ^{13}C NMR (150 MHz, H_2O/D_2O= 90/10), ppm: 30.7, 35.0, 35.8, 37.9, 40.0, 115.8, 117.8, 120.2, 128.0, 129.0, 129.1, 138.7, 140.4, 155.6, 157.6, 172.7. HRMS: calcd 513.268 ([M-H]$^+$); found 513.275.

Synthesis of compound 5

1-Naphthalenemethanethiol

1-Chlorometyl-naphtalene (5.28 g, 4.47 mL, 0.030 mol) was dissolved in 15 mL of ethanol (EtOH) under magnetic stirring. Thiourea (2.28 g, 0.030 mol, 1.0 eq.) was added and the reaction mixture was stirred for 2h at reflux temperature. The reaction mixture was then cooled at rt, filtered, washed with EtOH and evaporated under reduced pressure. The thiouronium salt was then dissolved in a 2M sodium hydroxide solution (5.0 mL, 9.5M) and stirred for 5 minutes. After that the reaction was quenched by HCl (4 M) at 0°C and then washed with DCM three times. The recovered organic phases were dried over sodium sulphate and evaporated under reduced pressure to afford a yellow-brownish solid (4.28 g, 82% overall yield). NMR spectra are fully consistent with those reported in literature.[28]

(1-Naphtylmethylthio)-4-(tert-butyl)-2,6-dinitrobenzene (13)

Compound **8**[19] (1.0 g, 2.5 mmol), 1-naphthalenemethanethiol (0.442 g, 2.5 mmol, 1.0 eq.) and DIEA (0.435 mL, 2.5 mmol, 1.0 eq.) were dissolved in anhydrous DCM (16.0 mL). The solution was stirred under nitrogen atmosphere for 16 h. Afterwards, the solution was washed with 10% citric acid solution and then with a saturated NaCl solution. The organic phase was dried over sodium sulfate. The crude was purified over silica gel (30 g; eluents: hexane and ethyl acetate, from 100:0 to 97:3), obtaining 0.876 g of thioether **13** (yield: 87.6 %). ^{1}H NMR (600 MHz, $CDCl_3$), δ: 1.38 (*s*, 9H), 4.68 (*s*, 2H), 7.36 (*t*, J = 8.0 Hz, 1H), 7.42 (*d*, J = 7.0 Hz, 1H), 7.50 (*t*, J = 7.0 Hz, 1H), 7.57 (*t*, J = 6.9 Hz, 1H), 7.79 (*s*, 2H), 7.80 (*d*, J = 8.3, 1H), 7.85 (*d*, J = 8.1 Hz, 1H), 8.12 (*d*, J = 8.4 Hz, 1H). ^{13}C NMR (150 MHz, $CDCl_3$), ppm: 31.3, 36.6, 40.8, 119.3, 124.0, 124.3, 126.0, 126.6, 127.2, 128.3, 129.0, 129.3, 129.7, 130.4, 131.8, 132.1, 134.5, 156.5, 156.7. HRMS: calcd 397.114 ([M-H]$^+$); found 435.218 ([M-K]$^+$).

(1-Naphtylmethylthio)-4-(tert-butyl)-2,6-diaminobenzene (15)

Compound **13** (0.850 g, 2.1 mmol), ammonium chloride (0.610 g, 11.4 mmol, 5.3 eq.) and zinc in powder (1.066 g, 16.3 mmol, 7.6 eq.) were suspended in methanol (25.0 mL) at 25.0 °C. The mixture was left under stirring in the dark and under argon atmosphere for 16h. The reaction mixture was evaporated and then filtered on a celite pad washing with toluene and ethyl acetate (1:1 v/v). The filtrate was concentrated *in vacuo* affording **15** as a white-pink solid with a quantitative yield. ^{1}H NMR (600 MHz, DMSO-d_6), δ: 1.17 (*s*, 9H), 4.20 (*s*, 2H), 5.01 (*bs*, 4H), 6.03 (*s*, 2H), 7.36-7.39 (*m*, 2H), 7.51-7.58 (*m*, 2H), 7.82 (*d*, J = 7.5 Hz, 1H), 7.92 (*d*, J = 7.8, 1H), 8.24 (*d*, J = 8.2 Hz, 1H). ^{13}C NMR (150 MHz, DMSO-d_6), ppm: 32.0, 35.1, 36.0, 98.4, 100.6, 100.1, 125.0, 126.5, 126.8, 127.2, 128.4, 128.7, 129.6, 132.1, 134.5, 135.1, 151.4, 153.8. HRMS: calcd 337.166 ([M-H]$^+$); found 337.155.

N,N'-(5-(tert-butyl)-2-((naphthalen-1-ylmethyl)thio)-1,3-phenylene)bis(3-guanidinopropanamide) (5)

Compound **15** (0.100 g, 0.301 mmol) was dissolved in anhydrous DMF (6.0 mL) under inert atmosphere. A mixture of 3-[*N*,*N*′-Bis(*tert*-butoxycarbonyl)guanidino]propionic acid (0.300 g, 0.903 mmol, 3.0 eq.), HBTU (0.342 g, 0.903 mmol, 3.0 eq.), HOBt (0.122 g, 0.903 mmol, 3.0 eq), DIEA (0.128 g, 0.993 mmol, 3.3 eq.) in anhydrous DMF (6.0 mL) was added to the reaction flask via cannula. The reaction mixture was stirred at room temperature for 16h. The reaction mixture was diluted with ethyl acetate and washed with brine three times. The organic layers were collected, dried over Na_2SO_4 and evaporated under reduced pressure. The brownish crude was then treated with a mixture of TFA/TIS/H_2O (95:2.5:2.5) at °0C and left stirring for 3h at RT. The solvent was removed under reduced pressure. The residue was purified by diethyl ether precipitation first, and then by reverse-phase chromatography (RP-C18, eluents: water 0.1% TFA (v/v), acetonitrile 0.1% TFA (v/v)), obtaining 0.130 g of **5** as a white solid (76 % yield, TFA salt). ^{1}H NMR (400 MHz, D_2O), δ: 1.28 (*s*, 9H), 2.24 (*t*, J = 6.6 Hz, 4H), 3.38 (*t*, J = 6.7 Hz, 4H), 4.24 (*s*, 2H), 6.69 (*d*, J = 7.5 Hz, 1H), 7.18 (*t*, J = 7.7 Hz, 1H), 7.57 (*bs*, 2H), 7.61 (*t*, J = 8.0 Hz, 1H), 7.65 (*t*, J = 8.0 Hz, 1H), 7.79 (*d*, J = 8.8 Hz, 1H), 8.19 (*d*, J = 8.7 Hz, 1H). ^{13}C NMR (100 MHz, D_2O), ppm: 30.1, 34.4, 34.8, 37.0, 118.6, 123.5, 125.3, 126.2, 126.6, 127.2, 128.1, 128.8, 132.7, 133.6, 139.9, 155.1, 171.7. HRMS: calcd 563.283 ([M-H]$^+$); found 562.292.

Synthesis of compound 6

4-[[Bis[[(1,1-dimethylethoxy)carbonyl]amino]methylene]amino]butanoic acid

4-Aminobutyric acid (1.20 g, 11.7 mmol) was dissolved in a solvent mixture of acetonitrile (ACN) and water (102 mL; 8% v/v water). At 0 °C, DIEA (4.44 mL, 25.5 mmol) was added, followed by the gradual addition of *N,N*′-Di-Boc-*1H*-pyrazole-1-carboxamidine (2.90 g, 9.35 mmol). The reaction mixture was stirred at room temperature for 4 hours. Upon completion, the reaction solvent was removed under reduced pressure, yielding an oily residue. The crude product was redissolved in diethyl ether (Et_2O) and washed three times with 0.2 M acetic acid (AcOH). The combined organic layers were dried over sodium sulfate (Na_2SO_4) and subsequently concentrated under reduced pressure. This process afforded a white solid (3.19 g, 78.9 % yield). The product was characterized by ^{1}H and ^{13}C NMR spectroscopy, confirming its identity as the Boc-protected guanidino acid. The spectra were consistent with previously reported data in the literature.[33]

N,N'-(5-(tert-butyl)-2-(phenethylthio)-1,3-phenylene)bis(4-guanidinobutanamide) (6)

Compound **10** (0.100 g, 0.333 mmol) was dissolved in anhydrous DMF (7.5 mL) under inert atmosphere. A mixture of 4-[[Bis [[(1,1-dimethylethoxy)carbonyl]amino]methylene]amino]butanoic acid (0.253 g, 0.733 mmol, 2.2 eq.), HBTU (0.278 g, 0.733 mmol,

2.2 eq.), HOBt (0.100 g, 0.733 mmol, 2.2 eq), DIEA (0.142 g, 1.10 mmol, 3.3 eq.) in anhydrous DMF (5.0 mL) was added to the reaction flask via a cannula. The reaction mixture was stirred at room temperature for 2 hours. The reaction mixture was diluted with ethyl acetate and washed with brine three times. The organic layers were collected, dried over Na_2SO_4 and evaporated under reduced pressure. The brownish crude was then treated with a mixture of TFA/TIS/H_2O (95:2.5:2.5) at °0C and left stirring for 2h at RT. The solvent was removed under reduced pressure. The residue was purified by diethyl ether precipitation first, and then by reverse-phase chromatography (RP-C18, eluents: water 0.1% TFA (v/v), acetonitrile 0.1% TFA (v/v)), obtaining 0.136 g of **6** as a white solid (74 % yield, TFA salt).^{1}H NMR (400 MHz, D_2O), δ: 1.32 (*s*, 9H), 1.95 (*q*, J = 7.07 Hz, 4H), 2.49 (*t*, J= 7.21 Hz, 4H), 2.73 (*t*, J = 6.99 Hz, 2H), 2.96 (*t,* J = 6.92 Hz, 2H), 3.25 (*t*, J = 6.9 Hz, 4H), 7.17 (*bd*, J = 7.51 Hz, 2H), 7.28 (*bt*, J = 7.15 Hz, 1H), 7.34 (*t*, J = 7.34 Hz, 2H), 7.59 (*bs*, 2H). ^{13}C NMR (100 MHz, D_2O), ppm: 24.0, 30.1, 32.8, 34.4, 35.4, 40.4, 120.0, 121.0, 126.5, 128.4, 128.6, 139.2, 139.9, 154.2, 156.7, 174.6. HRMS: calcd 555.315 ([M-H]$^+$); found 555.309.

Synthesis of N-19004-S (2)

N-19004 (**1**) as trifluoracetate salt, is dissolved in water (final concentration 10 mg/mL) and treated under stirring with a large excess of hydrogen peroxide solution (30.0 eq., 30% v/v) for 3h, at rt. The solution is then liophilized and **2** is obtained as a white powder with a quantitative yield. ^{1}H NMR (400 MHz, D_2O), δ: 1.29 (*s*, 9H), 2.12-2.33 (*bs*, 2H), 2.34-2.53 (*bs*, 2H), 3.19-3.49 (*bs*, 4H), 4.34 (*d*, J = 13.2 Hz, 1H), 4.68 (*d*, J = 13.2 Hz, 1H), 6.10 (*d*, J = 8.4 Hz, 1H), 7.47 (*s*, 1H), 7.58 (*quintet*, J= 6.5 Hz, 3H), 7.76-7.83 (*m*, 3H), 7.90 (*d*, J = 7.7 Hz, 1H). ^{13}C NMR (100 MHz, D_2O), ppm: 30.0, 34.8, 35.0, 36.9, 58.1, 120.1, 125.2, 126.8, 127.1, 127.5, 127.8, 128.0, 130.5, 132.6, 132.9, 156.7, 158.6, 171.7. HRMS: calcd 578.74 ([M-H]$^+$); found 578.82.

In vitro studies

Minimum Inhibitory Concentration (MIC) and Minimum Bactericidal Concentration (MBC) Determination

The antimicrobial activity of thioarylamide derivatives **1–6** was evaluated against a panel of ten Gram-positive and Gram-negative bacterial strains, listed in the table below:

Bacterial Strain	Strain Number	Other information
Burkholderia cenocepacia	*LMG 18863*	
Burkholderia multivorans	*LMG 17582*	
Burkholderia cenocepacia	*J2315*	
Pseudomonas aeruginosa	*AA2*	
Pseudomonas aeruginosa	*PAO1*	
Pseudomonas aeruginosa	*KK 27*	
Pseudomonas aeruginosa	*RP 73*	The strain was kindly provided by the Italian Cystic Fibrosis Research Foundation (FFC)
Enterococcus faecalis	ATCC® 29212	
Straphylococcus aureus	ATCC® 12600	
Straphylococcus aureus	ATCC® 29213	
Straphylococcus aureus	*MRSA* (WKZ-2)	The strain was kindly provided by the Italian Cystic Fibrosis Research Foundation (FFC)
Salmonella enterica serovar Typhimurium	ATCC® 14028	
Acinetobacter baumannii	ATCC® 19606	

Bacterial cultures were grown in Mueller–Hinton Broth (MHB) at 37 °C and harvested at mid-logarithmic growth phase. Cell suspensions were adjusted to approximately 2 × 10^6 CFU/mL and tested using the broth microdilution method, following Clinical and Laboratory Standards Institute (CLSI) guidelines.[63] Compounds were prepared as stock solutions and serially twofold diluted in Nutrient Broth (NB) to achieve final concentrations ranging from 0 to 200 μM in 96-well microtiter plates. Sterile phosphate-buffered saline (PBS) was used as the vehicle control (negative control), and fosfomycin was included as the positive control. Plates were incubated overnight at 37 °C. MIC values were defined as the lowest concentration of compound at which no visible bacterial growth was observed. To determine MBC values, aliquots from wells without visible growth were plated onto MHB agar and incubated for 24 h at 37 °C. The MBC was defined as the lowest compound concentration resulting in ≥90–95% bacterial killing.

Time-kill kinetic assays

Selected bacterial strains (*Staphylococcus aureus* ATCC® 12600, methicillin-resistant *Staphylococcus aureus* WKZ-2, *Pseudomonas aeruginosa* KK27, and *Pseudomonas aeruginosa* RP73) were treated with compounds **1-6** over time at concentrations corresponding to their MBC values (50 - 200 μM). To this aim, bacterial cells were diluted to 4 × 10^6 CFU/mL in 0.5× Nutrient Broth (NB) and mixed with solutions of compounds **1-6** (1:1 *v/v*) to reach the above concentrations. At defined time points (0, 15, 30, 60, 120, 180 and 1,440 min), samples were serially diluted, and each dilution was plated on tryptic soy agar (TSA) to count colonies after 20 h incubation at 37 °C.

Haemolytic activity

Human red blood cells (RBCs) were incubated with increasing concentrations (12.5–200 μM) of compounds **1-6** for 1 h at 37°C. Following the incubation, plates were centrifuged and supernatants from each well were transferred into new 96-well plates. Absorbance values were determined at 405 nm by using an automatic plate reader; the percentage of haemolysis was determined by comparison with control samples incubated in the presence of PBS (negative control) or of 1% (v/v) SDS in PBS solution (positive control, complete lysis).

Biofilm formation

Bacteria inoculum (*Staphylococcus aureus* ATCC® 12600, methicillin-resistant *Staphylococcus aureus* WKZ-2, *Pseudomonas aeruginosa* KK27, and *Pseudomonas aeruginosa* RP73) was grown overnight at 37 °C, and then diluted to 4 × 10^9 CFU/mL in 0.5X Mueller Hinton Broth (MHB) medium to be mixed 1:1 v/v with increasing concentrations of the compounds (final concentrations: 1.56–50 μM). N-19004 and N-19004-S were incubated at 37 °C for 24 h, in order to test the effects on biofilm formation. *Preformed Biofilm:* bacterial biofilms (*Staphylococcus aureus* ATCC® 12600, methicillin-resistant *Staphylococcus aureus* WKZ-2, *Pseudomonas aeruginosa* KK27, and *Pseudomonas aeruginosa* RP73) were formed for 24 h at 37 °C in 0.5X MHB, and then treated with 50 μM (in the case of *Pseudomonas aeruginosa* KK27 and *Pseudomonas aeruginosa* RP73) or 12.5 μM (in the case of *Staphylococcus aureus* ATCC® 12600 and methicillin-resistant *Staphylococcus aureus* WKZ-2) of each compound.

In vivo experiments

Immunocompetent C57BL/6NCrlBR male mice, 8-10 weeks old were purchased by Charles River (Calco, Italy) and transferred to San Raffaele Scientific Institute (Milan, Italy). The mice had been maintained under specific pathogen-free conditions and all procedures were carried out in the biosafety level 3 (BSL3) animal facility. Mice were maintained in sterile ventilated cages. Mice were fed with standard rodent autoclaved chow (VRFI, Special Diets Services, UK) and autoclaved tap water. Fluorescent lights were cycled 12h on, 12h off, and ambient temperature (23±1°C) and relative humidity (40-60%) were regulated.

Mice were infected as previously described[43,45] Briefly, mice were anesthetized by an intra-peritoneal (i.p) injection of ketamine (100 mg/kg) (Lobotor) and xylazine (10 mg/kg) (Rompun) in 0.9% NaCl and administered at a volume of 0.010 ml/g body weight. Mice were placed in supine position and the trachea was directly visualized by a ventral midline incision, exposed and intubated with a sterile, flexible 22-g cannula attached to a 1 ml syringe. An inoculum of 50 μl agar beads suspension of *Pseudomonas aeruginosa* MDR-RP73 embedding 1×10^6 colony-forming units (CFU) was implanted via the cannula into the lung, with both lobes inoculated. 47 mice were divided into 5 groups and starting soon after infection, mice were treated subcutaneously (s.c.) daily for seven days with N-19004 1 mg/kg, N19004 2,5 mg/kg, N19004 5 mg/kg, N19004 10 mg/kg or vehicle (sterile saline) using a dose volume of 100 μl per mouse. After infection, mortality and body weight were monitored. Animals were observed twice a day and those showed more than 25% of body weight loss and evidence of severe clinical disease, such as scruffy coat, inactivity, loss of appetite, poor locomotion, or painful posture, were sacrificed before the termination of the experiments with an overdose of carbon dioxide. At seven days post-infection (24 hours following the last treatment), mice were euthanized by CO_2 administration for microbiological analysis, bronchoalveolar lavage fluid (BALF) collection, and cell counts. BALF was extracted with a 22-gauge venous catheter by washing the lungs with 1 ml of RPMI 1640 (Euroclone) with protease inhibitor (Complete tablets, Roche Diagnostic) for three times. Quantitative bacteriology on BALF was performed by plating serial dilution on tryptic soy agar (TSA) (BD, Becton and Dickinson). Total cells recovered in the BALF were counted using an inverted light optical microscope after diluting an aliquot of the BALF 1:2 with Tuerk solution in a disposable counting chamber. BALF cells were centrifuged at 330 x g at 4° C for 8 minutes. The cell-free supernatants were stored at -80° C for potential additional analysis while the BALF cell pellet was resuspended in RPMI 1640 10% fetal bovine serum (FBS) at concentration of 1 x 10^6 cells/ml, and an aliquot of 150 μl was pipetted into the appropriate wells of the cytospin and centrifuged at 300 x g for 5 min, medium brake. Slides were then stained by Diff-Quik staining using a commercial kit (Medion Diagnostics, code: 726443), according to the manufacturer's instructions. A differential cell count was performed at an inverted light optical microscope. Lungs were aseptically removed and homogenized in 2 mL PBS with protease inhibitors (cOmplete™, Roche) using the homogenizer gentleMACS™ Octo Dissociator. 100 μl of the homogenates were serially diluted and plated on TSA plates for CFU counts. The remaining homogenates were then centrifuged at 16000x g for 30 minutes at 4°C, and the supernatants were stored at −80°C.

EPR experiments on bacterial model membranes

Materials

The zwitterionic lipid 1-palmitoyl-2-oleoyl-glycero-3-phosphocholine (POPC), the anionic lipid 1-palmitoyl-2-oleoyl-sn-glycero-3-phospho-(1'-rac-glycerol) (sodium salt) (POPG) and the spin-labeled phosphatidylcholines 1-palmitoyl-2-stearoyl-(*n*-doxyl)-sn-glycero-3-phosphocholine (*n*PC-SL) with n= 5, 7, 10, 14 were purchased from Avanti Polar Lipids (Alabaster, AL, USA). Lipopolysaccharide (LPS) from *Pseudomonas aeruginosa*, lipoteichoic acid (LTA) from *Staphylococcus aureus*, methanol, chloroform, sodium phosphate monobasic and dibasic, were provided by Merck (Darmstadt, Germany). 10 mM sodium phosphate buffer was prepared by dissolving proper amounts of the monobasic and the dibasic form in deionized water and the pH was adjusted to 7.4. In order to calculate the molar compositions of the lipid mixtures, the molar masses of LPS and LTA are needed.

The LPS molar mass was estimated by considering the different portions constituting the macromolecule, i.e., the lipid A, the core oligosaccharide and the *O*-chain. An average molecular weight for the lipid A portion was calculated from the data available in literature[64] where four variants are reported. Data for the core oligosaccharide domain were obtained from[65] and the molar mass was averaged on glycoform I and II. Finally, the *O*-antigen molecular weight was calculated from the data available in[66] for the serotype 10 of *Pseudomonas aeruginosa*, as it is the same serotype of the bacterium from which the commercial LPS was extracted. The calculated average molar mass is 6350 g mol^{-1}.

The commercial LTA mixture is also heterogenous in terms of molecular structure, containing a variety of homologues differing for the length of the acyl chains, the length of the polyglycerophosphate headgroup and the nature of the substituents in position two of the glycerol moieties.[67] By considering the average value of each source of variability, the average molar mass was estimated as 5490 g mol^{-1}.

Liposome preparation

To mimic the negative surface charge of bacterial membranes, a lipid mixture of POPC/POPG (80/20 mol/mol) was selected, as previously reported.[51] To obtain more relevant models for the Gram-positive bacterium *Staphylococcus aureus* and the Gram-negative bacterium *Pseudomonas aeruginosa*, pathogen-associated molecular patterns, LTA and LPS, were incorporated into the model membranes. Specifically, a lipid mixture of POPC/POPG/LTA (80/15/5 mol/mol) was chosen, with 5% LTA reflecting the average concentration found in Gram-positive bacteria.[68] For Gram-negative bacteria, an equivalent concentration of LPS was used, resulting in a model membrane composition of POPC/POPG/LPS (80/15/5 mol/mol). For liposome preparation, proper amounts of POPC and POPG were weighed in a round bottom glass tube and dissolved in a chloroform/methanol mixture (2/1 v/v). The organic solvent was then removed with a gentle nitrogen flux as required for the formation of a thin film. To add LPS or LTA, they were suspended in methanol (5 mg/mL) and sonicated with an amplitude of 59 kHz in a ultrasound water bath for 10 minutes. Proper volumes of these suspensions were then added onto the dry POPC/POPG film and methanol was removed with a gentle nitrogen flux. The samples were further dried under vacuum for at least two hours to guarantee the removal of all the organic solvent traces. Lipid films were hydrated with sodium phosphate buffer with or without N-19004 (1:0.2 lipid:N-19004 molar ratio). To promote Multilamellar Vesicles (MLVs) formation the process was performed at 40 °C (8 cycles alternating 30 s vortexing and 30 s rest). Samples were then sonicated with an amplitude of 59 kHz for 30 minutes prior to use to favor molecular dispersion of LPS or LTA within the lipid bilayer, adjusting a method reported in.[69] For EPR measurements, aliquots of *n*PC-SL solution in ethanol (1 % w/w) were added to the lipid mixture in organic solvent to obtain a final concentration of 2 % mol/mol over total lipids. For these experiments, MLVs suspensions were directly used.

Electron paramagnetic resonance (EPR)

EPR spectra of *n*PC-SL in MLVs suspensions in neat buffer or in the presence of N-19004 were recorded. Total lipid concentration in each sample was fixed at 10 mM. The experiments were performed on a 9 GHz Bruker Elexys E-500 spectrometer (Bruker, Rheinstetten, Germany). About 25 μL of the samples were loaded in glass capillaries and then placed in a standard 4 mm quartz sample tube. The sweep width was set at 100 G, the resolution at 1024 points, the modulation frequency at 100 kHz, the modulation amplitude at 1.0 G, the time constant at 20.5 ms and the incident power at 5.0 mW. To improve the signal to noise ratio, at least 8 scans were recorded for each sample. The spectra obtained were then quantitatively analyzed by determining the acyl chain order parameter, S, and the nitrogen isotropic hyperfine coupling constant, a'_N, as previously described.[69] For the lipid bilayers in the absence of N-19004, the effect of LPS and LTA on the spectra was quantified by calculating the differential order parameters, ΔS, and the differential nitrogen isotropic hyperfine coupling constants, $\Delta a'_N$, determined with respect to the values of S and a'_N obtained for POPC/POPG 80/20 mol/mol. For the sample in which N-19004 was included, the effect on the spectra was quantified by calculating the differential order parameters, ΔS, and the differential nitrogen isotropic hyperfine coupling constants, $\Delta a'_N$, determined with respect to the values of S and a'_N obtained for each lipid system in the absence of N-19004.

Scanning Electron Microscopy

Methicillin-resistant *Staphylococcus aureus* WKZ-2 and *Staphylococcus aureus ATCC® 12600* were incubated with 12.5 and 25 μM N-19004, while *Pseudomonas aeruginosa* KK 27 and *Pseudomonas aeruginosa* RP 73 with 25 and 50 μM N-19004 in NB 0.5X. Each bacterial strain was incubated at the concentration of 0.1 OD/mL with N-19004 for 16 h at 37 °C. Following incubation, bacteria were fixed in 2.5% glutaraldehyde. Following overnight incubation, bacteria were dehydrated with a graded ethanol series: 30% ethanol (1 × 10 min); 50% ethanol (1 × 10 min); 70% ethanol (1 × 10 min); 80% ethanol (1 × 10 min); 90% ethanol (1 × 10 min); 100% anhydrous ethanol (3 × 20 min). Bacteria deposited onto glass substrate were sputter coated with a thin layer of Au-Pd (Sputter Coater Denton Vacuum DeskV) to allow subsequent morphological characterization using a FEI Nova NanoSEM 450 at an accelerating voltage of 5 kV with Everhart Thornley Detector (ETD) and Through Lens Detector (TLD) at high magnification.

QUANTIFICATION AND STATISTICAL ANALYSIS

In vitro studies

All *in vitro* antimicrobial assays were performed in at least three independent experiments and data are presented as mean ± standard deviation (SD). Statistical significance between treated samples and untreated controls was assessed using the unpaired two-tailed Student's t-test. A p-value of less than 0.05 was considered statistically significant.

In vivo studies

All data are presented as mean ± S.E.M. Statistical analysis was performed on raw data using two-way analysis of variance (ANOVA) followed by Dunnett post-test for multiple comparisons for the analysis of body weights, and the one-way analysis of variance (ANOVA) followed by Dunnett post-test for comparison with the vehicle-treated group for the other read-outs. Outlier data, identified by Grubbs' test, were excluded from the analysis. A "p" value of <0.05 was considered to be statistically significant. Statistical analysis was performed using GraphPad software, version 10.0.